



รายงานการวิจัย

การสร้างแบบจำลองทางคณิตศาสตร์สำหรับการหาผลเฉลยเชิงตัวเลข
และผลเฉลยแม่นยำ ตรงของสมการ นาเวียร์ – สโตก เพื่ออธิบาย
พฤติกรรมกลศาสตร์ของไหล
(Mathematical modeling in fluid dynamics: numerical and
analytical solutions of the Navier-Stokes equations)

มหาวิทยาลัยเทคโนโลยีสุรนารี

ได้รับทุนอุดหนุนการวิจัยจาก
มหาวิทยาลัยเทคโนโลยีสุรนารี



รายงานการวิจัย

การสร้างแบบจำลองทางคณิตศาสตร์สำหรับการหาผลเฉลยเชิงตัวเลข
และผลเฉลยแม่นยำตรงของสมการ นาเวียร์ – สโตก เพื่ออธิบาย
พฤติกรรมกลศาสตร์ของไหล
(Mathematical modeling in fluid dynamics: numerical and
analytical solutions of the Navier-Stokes equations)

คณะผู้วิจัย

หัวหน้าโครงการ

รองศาสตราจารย์ ดร.นิโคไลย์ มอชกิน
สาขาวิชาคณิตศาสตร์
สำนักวิทยาศาสตร์

ผู้ร่วมวิจัย

ศาสตราจารย์ ดร.เชอร์เก้ เมเลชโก
อาจารย์ ดร.สายันต์ แก่นนาคำ
Prof. Dr. G.G.Chernyh

ได้รับทุนอุดหนุนการวิจัยจากมหาวิทยาลัยเทคโนโลยีสุรนารี ปีงบประมาณ พ.ศ. 2554
ผลงานวิจัยเป็นความรับผิดชอบของหัวหน้าโครงการวิจัยแต่เพียงผู้เดียว

สิงหาคม 2556

การสร้างแบบจำลองทางคณิตศาสตร์สำหรับการหาผลเฉลยเชิงตัวเลข
และผลเฉลยแม่นยำตรงของสมการ นาเวียร์ – สโตก เพื่ออธิบาย

พฤติกรรมกลศาสตร์ของไหล

(Mathematical modeling in fluid dynamics: numerical and
analytical solutions of the Navier-Stokes equations)

บทคัดย่อ

งานวิจัยนี้เกี่ยวกับบริเวณผสมเต็มรูปแบบแบบสองมิติยุบตัวลงในตัวกลางแบบแบ่งเป็นชั้นตามความหนาแน่นอย่างต่อเนื่อง งานวิจัยนี้เป็นการใช้การวิเคราะห์การคำนวณเชิงตัวเลขของพจน์แอดเวกทีฟในสมการนาเวียร์-สโตก ในการประมาณค่าของโอเบอเบค-บิวซิเนสส์ การเปรียบเทียบระหว่างการใช้แผนอัปวิน แผนจำกัดค่าฟังก์ชันที่ชื่อว่ามินมอด ซุปเปอร์บี แวนเลียร์ และโมโนโทไนซ์เซเตอร์ แผนหลายผลลู่ปรับตัวทางเดียวที่ชื่อ ENO3 และ SMIF และแผนหลายผลลู่ถ่วงน้ำหนัก WENO5 ได้ถูกเสนอในงานวิจัยนี้ ข้อมูลการทดลองจากห้องปฏิบัติการของ Wu ได้ถูกนำมาใช้ในการวัดเปรียบเทียบสมรรถนะ เพื่อเปรียบเทียบประสิทธิภาพของแนวทางทางการคำนวณเชิงตัวเลขต่าง ๆ ซึ่งพบว่าแผนจำกัดค่าฟังก์ชันจะให้การแพร่เชิงตัวเลขน้อยที่สุด แผน WENO5 ให้ความแม่นยำในการอธิบายความกว้างของบริเวณยุบตัวในเวลาที่แตกต่างกันได้มากกว่า และแผนทั้งหมดที่พิจารณาในงานวิจัยแสดงถึงแบบรูปที่เหมือนจริงสำหรับคลื่นโน้มถ่วงภายในที่ถูกสร้างโดยบริเวณยุบตัว

การสร้างแบบจำลองทางคณิตศาสตร์สำหรับการหาผลเฉลยเชิงตัวเลข
และผลเฉลยแม่นยำ ตรงของสมการ นาเวียร์ – สโตก เพื่ออธิบาย
พฤติกรรมกลศาสตร์ของไหล

**(Mathematical modeling in fluid dynamics: numerical and
analytical solutions of the Navier-Stokes equations)**

Abstracts

The problem of a two-dimensional fully mixed region collapsing in continuously density-stratified medium is considered. This research deals with the numerical treatment of the advective terms in the Navier-Stokes equations in the Oberbeck-Boussinesq approximation. Comparisons are made between the upwind scheme, flux-limiter schemes namely Minmod, Superbee, Van Leer and Monotonized Centred (MC), monotone adaptive stencil schemes namely ENO3 and SMIF, and weighted stencil scheme WENO5.

We used laboratory experimental data of Wu (J. Fluid Mech. , 1969, vol. 35) as a benchmark test to compare performance of different numerical approaches.

We found that flux limiter schemes have smallest numerical diffusion. The WENO5 scheme describes more accurately the width of collapse region variation with time. All considered schemes give realistic pattern of internal gravity waves generating by collapse region.

การสร้างแบบจำลองทางคณิตศาสตร์สำหรับการหาผลเฉลยเชิงตัวเลข
และผลเฉลยแม่นยำตรงของสมการ นาเวียร์ – สโตก เพื่ออธิบาย
พฤติกรรมกลศาสตร์ของไหล

**(Mathematical modeling in fluid dynamics: numerical and
analytical solutions of the Navier-Stokes equations)**

Abstracts

The problem of a two-dimensional fully mixed region collapsing in continuously density-stratified medium is considered. This research deals with the numerical treatment of the advective terms in the Navier-Stokes equations in the Oberbeck-Boussinesq approximation. Comparisons are made between the upwind scheme, flux-limiter schemes namely Minmod, Superbee, Van Leer and Monotonized Centred (MC), monotone adaptive stencil schemes namely ENO3 and SMIF, and weighted stencil scheme WENO5.

We used laboratory experimental data of Wu (J. Fluid Mech. , 1969, vol. 35) as a benchmark test to compare performance of different numerical approaches.

We found that flux limiter schemes have smallest numerical diffusion. The WENO5 scheme describes more accurately the width of collapse region variation with time. All considered schemes give realistic pattern of internal gravity waves generating by collapse region.

Contents

1	Introduction	4
1.1	Background and Significance	4
1.2	Performance of High Resolution Non-Oscillating Advection Schemes in the Context of the Flow Generated by a Mixed Region in a Stratified Fluid . .	5
1.3	Mathematical formulation	6
1.4	Numerical scheme	8
1.4.1	The high resolution numerical methods for transport equations . . .	9
1.4.2	Generalization for the multidimensional case	13
1.5	Results	13
1.5.1	Width, profiles and areas of collapsing region	14
1.5.2	Internal wave generated by collapsing region	17
1.6	Conclusions and future works	22
1.7	Acknowledgements	23



Chapter 1

Introduction

1.1 Background and Significance

There are two different types of stationary motion of bluff bodies in a fluid. The first type is a towed body. In the stationary motion regime external forces must affect the body. The second type is a self-propelled body. Many bodies (ships, submarines, living creatures, bacteria, microorganisms) are capable of self motion in a fluid. The term "self-propelled" means that a body moves because of the interaction between its boundary and the surrounding fluid and without the action of an external force. To realize such a motion regime, the body must have its own source of energy, i.e., the energy spent against the drag forces. In pure motion by self-propulsion the total net force and torque, external to the system body-fluid, acting on the body are zero. The forward force (thrust) that makes the body move is generated by the body itself and the motion is due to the interaction of the body's external surface and the fluid in which it is immersed.

The mathematical formulation of the problem of rigid body motion in a viscous liquid is described by Navier-Stokes equations. A numerical algorithm will be based on a projection method for solving the Navier-Stokes equations. The validation of our numerical algorithm will be done by a comparison with available numerical and experimental data. The results of various numerical experiments will be reported and discussed.

We found that it is necessary to use high order monotone approximation of convective terms in the Navier-Stokes equations. Due to this reason before to developed numerical code we have to verified and compare different approaches to approximate convective terms in governing equations. Analysis of high order, monotone finite-difference schemes has been done.

We compare flux-limiter, ENO3 and WENO5 approximation of convective terms. The two-dimensional flow generated by a local density perturbation (fully mixed region) in stratified fluid is considered. In order to describe accurately the sharp discontinuity in density at the edge of the mixed region, monotone schemes of high order of approximation are required. Although a great variety of methods have been developed on the last decades, there remains the question of which method is the best. This present paper deals with the numerical treatment of the advective terms in the Navier-Stokes equations in the Oberbeck-Bousinesq approximation. Comparisons are made between the upwind scheme, flux-limiter schemes namely Minmod, Superbee, Van Leer and Monotonized Centred (MC), monotone adaptive stencil schemes namely ENO3 and SMIF, and the weighted stencil scheme WENO5. We used the laboratory experimental data of Wu as a benchmark test to compare the performance of the various numerical approaches. We found that the flux limiter schemes have the smallest numerical diffusion. On the other hand,

the WENO5 scheme describes the variation of the width of the collapsing region over time most accurately. All considered schemes give realistic patterns of internal gravity waves generated by the collapsing region.

1.2 Performance of High Resolution Non-Oscillating Advection Schemes in the Context of the Flow Generated by a Mixed Region in a Stratified Fluid

The dynamics of a mixed region in density stratified fluids plays an important role in numerous geophysical and engineering applications, and is responsible for the transport of heat, nutrients and pollutants in the oceans and the atmosphere, as well as in various technical devices. In the ocean, for example, turbulent mixing can be caused by tidal flow over bottom topography, by breaking of internal waves or by a body traveling through the oceanic thermocline. Since the mixed fluid region has excess potential energy over its surroundings, the fluid must move towards a new stable equilibrium state; this results in the collapse of the mixed region. The character of this collapse is generally complicated and depends on various parameters including the shape and dimensions of the mixed region, the level of mixing and the background stratification profile. A correct representation of the mixing zone dynamics within a linearly and nonlinearly stratified fluid is a major problem in geophysical and oceanography research.

A number of geophysical phenomena and a number of technical problems related to a flow generated by a local density perturbation in a stratified fluid were studied by [41, 1, 2, 33, 3] and [4]. For example, because the turbulent wake behind a body traveling through a stratified fluid is very slender in the direction of body motion, the flow field induced by wake and the internal waves can be adequately described by studying the collapse of a non-turbulent mixed region in a stratified medium, as investigated by [24], [8], [3], [9] and [10].

There are numerous studies focusing on locally homogeneous perturbations of density fields (fully mixed regions). Experimental work on this problem has been done by [11]. To the best of the author's knowledge, [12] was the first person who solved the full nonlinear equations numerically for the case of a sharp discontinuity in the density field at the mixed region edge. He obtained gross corroboration with the experiment of [11] in terms of wave patterns and horizontal size of the mixed region for large time values. The properties of the internal wave patterns are well described in [13] for the case of laminar collapse of the mixed region having various initial density perturbations in a linearly stratified medium. This problem was used by several researchers as a benchmark test in order to assess the performance of numerical algorithms, i.e. [25] and [6]. In a paper of [14], the idea of a nondiffusing passive scalar was used to study the shape of the mixed region over a time period. The methods for localization of singularities by [15] was utilized to define the location of the mixed region edge.

Variable density incompressible viscous flow presents a difficulty for satisfying the property of mass conservation in two respects. On the one hand, the mass density of each fluid particle must remain unchanged during the fluid motion, whatever the level of unsteadiness and mixing. On the other hand, the velocity field must satisfy the incompressibility constraint which reflects the inability of pressure to do compression work. These two important physical characteristics are fully described by the set of the incompressible Navier-Stokes equations augmented by the advection equation for the density. The sharp

front/discontinuities are transported from one location to another, described very well by an advection model. The problem of accurately modeling advection is not limited to the area of geophysical models, and a number of review articles are available in the literature. In regions with large substance gradients and/or velocities, the advection schemes used in many models (upwind-first order, central differences-second order) lead to significant diffusion and/or under- and overshoot of substance values. To describe a sharp discontinuity in the density field at the mixed region edge accurately enough, schemes with high-order approximation of advection terms are required. Godunov's theorem states that any linear monotonic advection scheme can provide no more than first-order accuracy. Therefore, there is a need to apply higher order accuracy nonlinear numerical schemes devised for numerical solutions of conservation laws which support discontinuous solutions.

Computational experience demonstrates that numerical solutions reproduce the physical phenomenon better if they satisfy additional properties such as conservativeness, monotonicity, maximum principle, diminishing total variation and other properties. Many methods match additional requirements; examples are the Lax-Wendroff, Lax-Friedrichs, flux corrected transport (FCT) methods of Boris-Book and Zalesak, slope limiter methods of Van Leer, essentially non-oscillatory (ENO) schemes of Harten-Shu-Osher and total variation diminishing schemes (TVD). There are some books, for example [16, 17], that discuss many of the classical schemes as well as the flux corrected transport schemes following the work of [18]. Even though there are very few theoretical results about the properties of such schemes in multidimensional and nonlinear cases, in practice these schemes are very robust and stable, and are used in many practical applications. However, there is always the question of what scheme is the best choice, the answer to which is usually problem dependant.

Analysis of the known literature on numerical modeling of flow generated by collapse of a mixed region in a linearly stratified medium shows that there are no studies on the applicability of high-order resolution advection finite-difference schemes to this problem with discontinuity in the density field. A sufficiently complete list of references and a comprehensive overview of research related to numerical modeling of local density perturbed dynamics can be found in [8].

This study has two objectives: the first is to highlight the high-order upwind schemes as an effective methodology for solving problems of mixed region collapse in stratified media, and the second is to improve the predictability of numerical modeling of problems with sharp discontinuities in the density field.

1.3 Mathematical formulation

The governing equations are the Navier-Stokes equations in the Oberbeck-Boussinesq approximation:

$$\frac{\partial u}{\partial t} + u \frac{\partial u}{\partial x} + w \frac{\partial u}{\partial z} + \frac{1}{\rho_0} \frac{\partial p_1}{\partial x} = \nu \left(\frac{\partial^2 u}{\partial x^2} + \frac{\partial^2 u}{\partial z^2} \right), \quad (1.1)$$

$$\frac{\partial w}{\partial t} + u \frac{\partial w}{\partial x} + w \frac{\partial w}{\partial z} + \frac{1}{\rho_0} \frac{\partial p_1}{\partial z} = \nu \left(\frac{\partial^2 w}{\partial x^2} + \frac{\partial^2 w}{\partial z^2} \right) - g \frac{\rho_1}{\rho_0}, \quad (1.2)$$

$$\frac{\partial u}{\partial x} + \frac{\partial w}{\partial z} = 0, \quad (1.3)$$

$$\frac{\partial \rho}{\partial t} + u \frac{\partial \rho}{\partial x} + w \frac{\partial \rho}{\partial z} = 0. \quad (1.4)$$

Here ν is the coefficient of kinematic viscosity, u and w are the components of velocity in x and z directions of Cartesian coordinates as shown in Figure 1.1, $\rho = \rho(x, z, t)$ is the density, $\rho_1(x, z, t) = \rho(x, z, t) - \rho_s(z)$, $\rho_s = \rho_s(z)$ is the density of undisturbed media, $\rho_0 = \rho_s(0)$, p_1 is the deviation of pressure from hydrostatic pressure, and g is the gravitational acceleration. The stratification is assumed to be linear and stable, i.e. $d\rho_s/dz = -a\rho_0$, where $a = \text{const} > 0$.

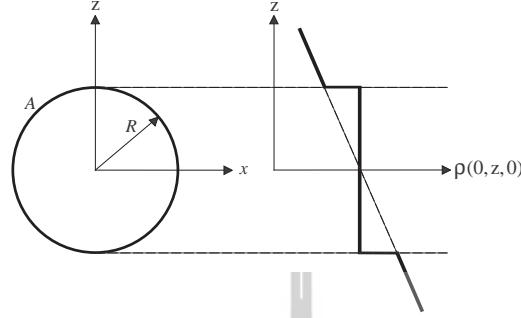


Figure 1.1: A circular mixed region with full mixing

The boundary and initial conditions are

$$\rho_1 = 0, \quad u = w = 0, \quad \text{if } x^2 + z^2 \rightarrow \infty, \quad t \geq 0, \quad (1.5)$$

$$\rho = \begin{cases} \rho_0, & \text{if } (x, z) \in A, \quad t = 0, \\ \rho_s(z), & \text{if } (x, z) \notin A, \quad t = 0, \end{cases} \quad (1.6)$$

$$u = w = 0, \quad \text{if } -\infty < x, z < \infty, \quad t = 0. \quad (1.7)$$

Here A is the domain of totally mixed fluid, in our particular case, $A = \{(x, z) : x^2 + z^2 \leq R^2\}$. System of equations (1.1)–(1.4), initial and boundary conditions (1.5)–(1.7) can be cast in a dimensionless form by using R as the scale of length (the mixing zone radius), and Vaisala-Brunt period, $T = 1/\sqrt{ag}$, as time scale: besides, the representation $\rho = \rho_0 a R \bar{\rho}$ ($\bar{\rho}$ denotes dimensionless density) is used. As a result, the value $1/Re = \nu T/R^2$ appears in the dimensionless equations instead of ν , and 1 instead of g .

To study the history of the shape of the mixed region, the idea of non-diffusing passive scalar will be used. The transport equation of passive scalar is solved together with system (1.1)–(1.4)

$$\frac{\partial C}{\partial t} + u \frac{\partial C}{\partial x} + w \frac{\partial C}{\partial z} = 0, \quad (1.8)$$

with initial and boundary conditions

$$C(0, x, z) = \begin{cases} C_0 = \text{const}, & \text{if } (x, z) \in A, \\ 0, & \text{if } (x, z) \notin A, \quad t = 0, \end{cases} \quad (1.9)$$

$$C(t, x, z) = 0, \quad \text{if } x^2 + z^2 \rightarrow \infty, \quad t > 0. \quad (1.10)$$

Here $C(t, x, z)$ is the concentration of the passive scalar. The edge of the mixed region can be defined as the location of the discontinuity in passive scalar concentration. The motion of passive Lagrangian particles is also used to visualize the flow.

1.4 Numerical scheme

A finite difference scheme is used for the numerical solution of the governing equations. Variables are discretized on a uniform rectangular grid of mesh size Δx and Δz in the horizontal and vertical directions, respectively, and the time step is denoted by Δt . For the sake of simplicity of a numerical algorithm representation, the system of equations is recast in the following form,

$$\mathbf{u}_t + (\mathbf{u} \cdot \nabla)\mathbf{u} = -\nabla p + \frac{1}{Re}\Delta\mathbf{u} - \rho_1\mathbf{z}, \quad (1.11)$$

$$\rho_t + (\mathbf{u} \cdot \nabla)\rho = 0, \quad (1.12)$$

$$\nabla \cdot \mathbf{u} = 0, \quad (1.13)$$

where ρ is the density, \mathbf{u} is the velocity vector, and \mathbf{z} is the unit vector in direction opposite to the gravitational force. In two dimensional space the staggered grid is shown in Figure 1.2 and the following notations $\mathbf{u} = (u, w)$, $\mathbf{q} = (u, w, \rho) = (\mathbf{u}, \rho)$ are used. The notations in Figure 1.2 are described as follows: let Ω_{ij} be the (i, j) -th grid cell $[x_{i-1/2}, x_{i+1/2}] \times [z_{j-1/2}, z_{j+1/2}]$, the "edge velocities" $u_{i\pm 1/2, j}$ and $w_{i, j\pm 1/2}$ are the velocity components at the midpoints of the interfaces $(x_{i\pm 1/2}, z_j)$ and $(x_i, z_{j\pm 1/2})$, and the centered values \mathbf{Q}_{ij}^n and \mathbf{U}_{ij}^n represent an approximation to the cell average of \mathbf{q} and \mathbf{u} at the current time level $t^n = t^{n-1} + \Delta t$,

$$\mathbf{Q}_{ij}^n = \frac{1}{\Delta x \Delta z} \int_{\Omega_{ij}} \mathbf{q}(x, z, t) dx dz, \quad \mathbf{U}_{ij}^n = \frac{1}{\Delta x \Delta z} \int_{\Omega_{ij}} \mathbf{u}(x, z, t) dx dz. \quad (1.14)$$

The projection method for the above system (1.11)–(1.13) can be stated as follows:

- Step I: Use the centered values $\mathbf{Q}^n = (U^n, W^n, \rho^n)$ and edge values $\mathbf{u}^n = (u^n, w^n)$ to solve the advection equation

$$\frac{\tilde{\mathbf{Q}} - \mathbf{Q}^n}{\Delta t} + \mathbf{u}^n \cdot \nabla \mathbf{Q}^n = 0. \quad (1.15)$$

This is solved on a finite volume grid using the explicit high-resolution monotone algorithm. The resulting solution is $\tilde{\mathbf{Q}} = (\tilde{U}, \tilde{W}, \rho^{n+1}) = (\tilde{\mathbf{U}}, \rho^{n+1})$.

- Step II: Use a Crank-Nicolson discretizing for diffusion

$$\frac{\mathbf{U}^* - \tilde{\mathbf{U}}}{\Delta t} = \frac{1}{2Re}(\nabla^2 \mathbf{U}^n + \nabla^2 \mathbf{U}^*) - \rho_1^{n+1} \mathbf{z}. \quad (1.16)$$

Spacial centered finite differences are used to approximate diffusive terms in above equation. This gives the intermediate velocity $\mathbf{U}^* = (U^*, W^*)$ at the cell center.

- Step III: Obtain the edge velocity by

$$\mathbf{u}^{n+1} = \mathbf{u}^* - \mathcal{G}(\Delta t \phi^{n+1}), \quad (1.17)$$

where the function ϕ denotes the scalar potential in the Hodge decomposition theorem, $\mathbf{u}^* = (u^*, w^*)$ is the average of the adjacent \mathbf{U}^* ,

$$u_{i-1/2, j}^* = \frac{1}{2}(U_{i-1, j}^* + U_{i, j}^*), \quad w_{i, j-1/2}^* = \frac{1}{2}(W_{i, j-1}^* + W_{i, j}^*),$$

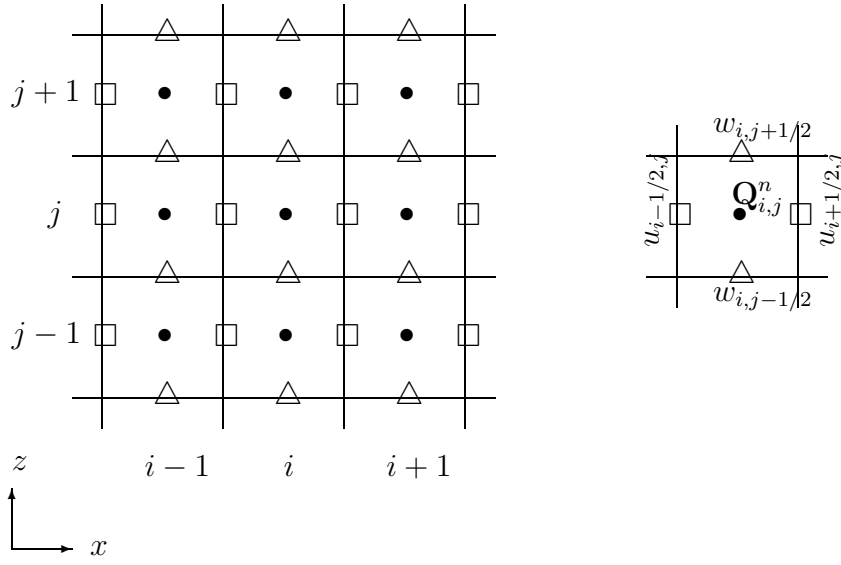


Figure 1.2: Staggered Grid: $\square - u$, $\triangle - w$ and $\bullet - \mathbf{Q}$ (or \mathbf{U})

and \mathcal{G} is the discrete gradient operator defined as follows,

$$\mathcal{G}\phi_{i,j} = \left(\frac{\phi_{i,j} - \phi_{i-1,j}}{\Delta x}, \frac{\phi_{i,j} - \phi_{i,j-1}}{\Delta z} \right).$$

The update (1.17) requires the values ϕ^{n+1} , which can be obtained by solving a discrete Poisson problem $\mathcal{D}\mathcal{G}(\Delta t\phi)_{ij}^{n+1} = (\mathcal{D}\mathbf{u}^*)_{ij}$, where \mathcal{D} is the discrete divergency operator defined as follows,

$$(\mathcal{D}\mathbf{u})_{i,j} = \frac{u_{i+1/2,j} - u_{i-1/2,j}}{\Delta x} + \frac{w_{i,j+1/2} - w_{i,j-1/2}}{\Delta z}.$$

The value ϕ^{n+1} is obtained by the fractional step method with stabilizing correction [49]. The pressure p^{n+1} can be obtained from ϕ^{n+1} through the relationship [19],

$$p^{n+1} = \phi^{n+1} - \frac{\Delta t}{2Re} \nabla^2 \phi^{n+1}.$$

- Step IV: In the final step, we update the cell-centered velocity by

$$U_{i,j}^{n+1} = U_{i,j}^* - \frac{\Delta t}{2} (\phi_{i+1,j}^{n+1} - \phi_{i-1,j}^{n+1}) / (\Delta x),$$

$$W_{i,j}^{n+1} = W_{i,j}^* - \frac{\Delta t}{2} (\phi_{i,j+1}^{n+1} - \phi_{i,j-1}^{n+1}) / (\Delta z).$$

This completes one time step. Go to Step I for next time step.

1.4.1 The high resolution numerical methods for transport equations

A monotone scheme of high order of approximation is required to describe the discontinuity in density at the edge of the mixed region with sufficient accuracy. For simplicity, a brief illustration of the algorithms used, we consider the one-dimensional scalar advection equation in a specified incompressible velocity field $u(t, x)$

$$\frac{\partial Q}{\partial t} + \frac{\partial uQ}{\partial x} = 0, \quad (1.18)$$

where Q is a conservative quantity which can be a velocity component, density or passive scalar concentration function. The flux of quantity Q is denoted by F . A regular spacial grid is defined by the points $x_i = i\Delta x$, $i = 0, 1, \dots, N$ also called the cell centers. The time step is denoted by Δt . To maintain the conservative property of (1.18) the numerical flux $\widehat{F}(x, t)$ is implicitly defined by

$$F(x, t) = \frac{1}{\Delta x} \int_{x-\Delta x/2}^{x+\Delta x/2} \widehat{F}(x, t) dx,$$

such that the derivative $\partial F/\partial x$ is calculated exactly by the following formula:

$$\frac{\partial F}{\partial x}(x, t) = \frac{\widehat{F}(x + \Delta x/2, t) - \widehat{F}(x - \Delta x/2, t)}{\Delta x}.$$

Hence, discretization of equation (1.18) is obtained in the flux form and can be expressed explicitly in time as

$$Q_i^{n+1} = Q_i^n - \frac{\Delta t}{\Delta x} \left[\widehat{F}_{i+1/2}^n - \widehat{F}_{i-1/2}^n \right], \quad (1.19)$$

where n is the time level, $t^n = n\Delta t$, $Q_i^n = Q(x_i, t^n)$ and $\widehat{F}_{i\pm 1/2}^n$ are the Q fluxes through the right and left boundaries of the grid cell, respectively. In the sections below, the different numerical approximations of the $\widehat{F}_{i\pm 1/2}^n$ in (1.19) that are used in this work are presented. These include four flux-limiter methods, two adaptive stencil methods, and one weighted stencil method.

Flux-limiter

Flux-limiter schemes satisfy many of the requirements of a good advection scheme. In particular, they are total variation diminishing (TVD), mass conservative and less diffusive than the simpler schemes (see for example, Harten [28] and LeVeque [30]).

The accuracy of finite discretization is mainly related to the computation of the cell-face fluxes $\widehat{F}_{i+1/2}^n$. The most straightforward approximation to $\widehat{F}_{i+1/2}^n$ is certainly $\widehat{F}_{i+1/2}^n = 0.5u_{i+1/2}^n(Q_i^n + Q_{i+1}^n)$. This expression gives an approximation of the partial derivative $\partial uQ/\partial x$ by central differences. This method leads to the appearance of spurious oscillations in the numerical solution. One strategy to avoid nonphysical oscillations and excessive numerical diffusion is the hybrid method which uses the second order numerical flux in smooth regions and limits the solution in vicinity of discontinuities by using the monotonic upwind method in these regions. This procedure is carried out by introducing a flux-limiter based on the local gradient of the solution. We write the interface value $Q_{i+1/2}^n$ as the sum of the diffusive first order upwind term and an ‘‘anti-diffusive’’ one. The higher order antidiffusive part is multiplied by the flux limiter, which depends locally on the nature of the solution by means of the non-linear function $\theta_{i+1/2}$. This function is expressed by the slope ratios at the neighborhood of the interfaces in the upwind direction,

$$\theta_{i+1/2} = \begin{cases} \frac{Q_i^n - Q_{i-1}^n}{Q_i^n - Q_{i-1}^n} = \theta_{i+1/2}^+ & \text{if } u_{i+1/2}^n \geq 0, \\ \frac{Q_{i+2}^n - Q_{i+1}^n}{Q_{i+1}^n - Q_i^n} = \theta_{i+1/2}^- & \text{if } u_{i+1/2}^n < 0. \end{cases} \quad (1.20)$$

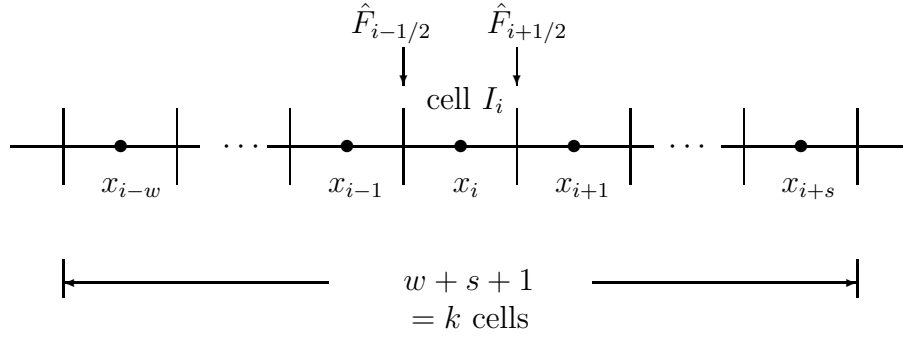


Figure 1.3: Stencil $S_i^{(w)} = \{I_{i-w}, \dots, I_{i-1}, I_i, I_{i+1}, \dots, I_{i+s}\}$

Introduction of this new parameter namely (θ) and the limiter function Ψ , leads to the flux limiter version of the hybrid scheme as

$$Q_{i+1/2}^n = \begin{cases} Q_i^n + \frac{1}{2}(Q_{i+1}^n - Q_i^n)\Psi(\theta_{i+1/2}^+) & \text{if } u_{i+1/2}^n \geq 0, \\ Q_{i+1}^n - \frac{1}{2}(Q_{i+1}^n - Q_i^n)\Psi(\theta_{i+1/2}^-) & \text{if } u_{i+1/2}^n < 0. \end{cases} \quad (1.21)$$

The interface value $Q_{i-1/2}^n$ is obtained from $Q_{i+1/2}^n$, by replacing the index i with $i - 1$. From Eq. (1.21), one can see that if $\Psi = 0$ we find the upwind scheme, and if $\Psi = 1$ the scheme is reduced to the central one. The following limiter functions are used in this study [30]:

$$\begin{aligned} \text{Minmod} : \Psi(\theta) &= \max(0, \min(1, \theta)), \\ \text{Superbee} : \Psi(\theta) &= \max(0, \min(1, 2\theta), \min(2, \theta)), \\ \text{van Leer} : \Psi(\theta) &= (\theta + |\theta|)/(1 + |\theta|), \\ \text{MC} : \Psi(\theta) &= \max(0, \min(\frac{1 + \theta}{2}, 2, 2\theta)). \end{aligned} \quad (1.22)$$

The Minmod and Superbee limiters were introduced by Roe [38] and Roe and Sidilkover [39]. The van Leer limiter was introduced in van Leer [42] and the monotized central (MC) limiter was also introduced by van Leer in a later paper [43].

Adaptive stencil (AS) methods

As depicted in Figure 1.3, a formal definition of a cell (I_i) and a stencil (S_i) in the context of high resolution numerical methods is as follows: $I_i \equiv [x_{i-1/2}, x_{i+1/2}]$, $S_i^{(w)} = [I_{i-w}, I_{i-w+1}, \dots, I_i, I_{i+1}, \dots, I_{i+s}]$, $w = -1, 0, 1, \dots, k - 1$ where w and s represent the number of cells taken to the left and right of cell i , respectively, also referred to as the left and right stencil shift. The order of accuracy k on each stencil is related to w and s via the following relation: $k = w + s + 1$. If the same stencil is used for discretizing the partial differential equation at all grid cells I_i , then it is known that fixed stencil methods of second or higher order suffer from nonphysical oscillations in the regions of discontinuity and in the neighborhood of steep fronts. As indicated by Shu [40], the paper of Harten *et al.* [29] directed the research toward an alternative approach, the adaptive stencil methods. The idea behind the adaptive stencil methods is to keep the total number of cells in the stencil constant, and to change the left shift w of the stencil if necessary with the coordinate x_i in order to avoid including the cell with the discontinuity in the interpolating polynomial. Thus, from a number of candidate stencils at each location x_i , the optimum stencil that results in the elimination of the numerical oscillation is chosen to approximate the flux.

SMIF method

The first adaptive stencil method used in this work is the hybrid monotonic difference scheme developed in Gushchin *et al.* [26, 27], and Belotserkovskii [7] for the numerical simulation of fluid flows with large gradients of hydrodynamic parameters. The splitting on physical factors method for incompressible fluid flows (SMIF) is based on a combination of the modified central difference scheme MCDS and the modified upwind difference scheme MUDS with special switch condition. The splitting scheme is similar to the famous SMAC method of Amsden and Harlow [5], and to one of the approaches suggested in Fortin *et al.* [23]. It was shown that this hybrid scheme comes nearest to the third order schemes (Gushchin and Konshin [26]).

Essentially non oscillatory (ENO) scheme

The second adaptive stencil method used in this work is the third order essentially non oscillatory (ENO3) scheme. For the ENO scheme, as shown in Figure 1.3, k candidate stencils can be defined at each cell I_i . On each of these stencils a k -th order interpolation polynomial can be constructed:

$$\widehat{F}_{i+1/2}^{(w)} = \sum_{j=0}^{k-1} c_{w,j}^{(k)} F_{i-w+j}, \quad w = 0, \dots, k-1,$$

where $k = 3$ for the ENO3 scheme. The coefficients $c_{w,j}^{(k)}$ can be found in Shu [40] for a fixed uniform grid. Smoothness indicators are used to estimate the smoothness of the solution. For $k = 3$ the smoothness indicators are given in Shu [40]. The stencil on which the interpolation is smoothest is then used for approximating the flux $\widehat{F}_{i+1/2}$.

Weighted stencil methods (WENO)

The WENO scheme is a weighted stencil method in which the idea is once again to define a number of candidate stencils at each grid location, but instead of selecting one of them for calculating the numerical flux, a convex combination of all candidate stencils is used. The advantage is that this method possesses k -th order accuracy in the vicinity of discontinuities or steep fronts, and $(2k - 1)$ -th order accuracy in smooth regions, where $k = w + s + 1$.

WENO5 scheme

The finite difference WENO5 scheme uses the same idea of applying ENO3 to construct cell faces of numerical fluxes. However, WENO5 uses a combination of 3 stencils $\{S_i^{(0)}, S_i^{(1)}, S_i^{(2)}\}$ or $\{S_i^{(-1)}, S_i^{(0)}, S_i^{(1)}\}$ for constructing interpolating polynomials depending on upwinding. If $(u_{i+1/2} > 0)$ (positive direction), the construction of $\widehat{F}_{i+1/2}$ based on the 5th-order WENO5 scheme can be expressed as

$$\widehat{F}_{i+1/2} = \sum_{w=0}^2 \omega_w f_{i+1/2}^{(w)}, \quad \omega_w = \frac{\alpha_w}{\sum_{l=0}^2 \alpha_l}, \quad \alpha_w = \frac{d_w}{(\epsilon - \beta^{(w)})^2}, \quad (1.23)$$

$$(d_0, d_1, d_2) = \left(\frac{3}{10}, \frac{3}{5}, \frac{1}{10} \right),$$

where $f_{i+1/2}^{(w)}$ approximates $\widehat{F}_{i+1/2} = (uQ)_{i+1/2}$ using cell stencil $S_i^{(w)}$, $w = 0, 1, 2$ as shown in (1.24). The parameter $\epsilon = 10^{-6}$ is used to avoid a zero denominator.

$$\begin{aligned} f_{i+1/2}^{(0)} &= \frac{1}{3}F_i + \frac{5}{6}F_{i+1} - \frac{1}{6}F_{i+2}, & f_{i+1/2}^{(1)} &= -\frac{1}{6}F_{i-1} + \frac{5}{6}F_i + \frac{1}{3}F_{i+1}, \\ f_{i+1/2}^{(2)} &= \frac{1}{3}F_{i-2} - \frac{7}{6}F_{i-1} + \frac{11}{6}F_i, \end{aligned} \quad (1.24)$$

with the smoothness indicators $\beta^{(w)}$ given by

$$\begin{aligned} \beta^{(0)} &= \frac{13}{12}(F_i - 2F_{i+1} + F_{i+2})^2 + \frac{1}{4}(3F_i - 4F_{i+1} + F_{i+2})^2, \\ \beta^{(1)} &= \frac{13}{12}(F_{i-1} - 2F_i + F_{i+1})^2 + \frac{1}{4}(F_{i-1} - F_{i+1})^2, \\ \beta^{(2)} &= \frac{13}{12}(F_{i-2} - 2F_{i-1} + F_i)^2 + \frac{1}{4}(F_{i-2} - 4F_{i-1} + 3F_i)^2. \end{aligned} \quad (1.25)$$

1.4.2 Generalization for the multidimensional case

The generalization of the above finite-difference schemes to 2D and 3D problems is easily performed for convective terms as splitting mode in each one-dimensional direction. This way of extending the finite difference schemes is very simple and efficient, and hence is widely used in applications. However, such a generalization of the scheme to the multidimensional case can be only second order accurate for general nonlinear systems regardless of the order of accuracy in the one-dimensional procedure (as pointed out by Zhang *et al.* [50]).

1.5 Results

In this section we are comparing the performance of the high-order upwind schemes for the unsteady problem of the collapse of a mixed region in a linearly stratified fluid. Due to symmetry, the solution of problem (1.1)-(1.7) was sought in the first quadrant ($x \geq 0$ and $z \geq 0$) of the plane (x, z) with the symmetry conditions at $x = 0$ and $z = 0$. When solving the problem considered, the zero conditions at infinity were shifted and formulated at the boundary of a sufficiently large rectangular region. Variables are discretized on a uniform rectangular grid of mesh size Δx and Δz in the horizontal and vertical directions, respectively. The three different grids with $\Delta x = \Delta z = 0.1$, $\Delta x = \Delta z = 0.05$, and $\Delta x = \Delta z = 0.025$, are used to estimate rate of convergence. Order of accuracy is based on the ratio of errors from the two finest grids. The convergence rate of the flux-limiter schemes is a little less than 2^{nd} -order. The convergence rate of SMIF, ENO3 and WENO5 is a little better than 2^{nd} -order. These results are in agreement with the comments of Zhang *et al.* [50] that the ENO and WENO schemes are only 2^{nd} -order accurate for a general nonlinear system, regardless of the order of accuracy in the one dimensional reconstruction procedure. The selection of a suitable domain size is based on a straightforward analysis in which the size of the domain is systematically increased until its effect on prediction becomes small. A domain of length $x_* \simeq 10R$ and height $z_* \simeq 4R$ was found reasonable for the time interval considered. In his laboratory experiment, Wu [48] examined in detail the collapse of the original mixed region and the growth and propagation of internal waves. The process of collapse can be divided into initial, principal and final collapse stages. At the first two stages, the collapse is

a gravitation flow phenomenon. Empirical formulae have been derived to describe the process of the first two stages. A nearly constant rate of collapse is found for the initial stage. The rate of wake collapse slows down gradually at the principal collapse stage. At the final stage, the collapse slows down even further with increasing viscous effects. We used the data of Wu [48] as a benchmark test to compare performance of the different numerical approaches.

1.5.1 Width, profiles and areas of collapsing region

The profiles of the collapsing region were traced from the evolution of the passive scalar concentration and from the evolution of Lagrangian particles' positions. The finite difference schemes have different smearing of the density and passive scalar concentration discontinuities. The best way to define the evolution of mixing zone size is to draw and analyze profiles of passive scalar concentration at different transects. These results are shown clearly in Figures 1.4 and 1.5 in which we present a transect $z = 0.5\Delta z$ of the numerical solution for passive scalar concentration. Figure 1.4 shows the graphs of transect $z = 0.5\Delta z$ for different moments of time. Here we compare upwind (no flux-limiter) scheme with four flux-limiter schemes given by equations (1.22). The first order upwind scheme smears the solution too much (see lines marked by circle signs). The limiter schemes reduce the numerical diffusion as compared to the upwind scheme. Comparing the performance of MC and van Leer limiters (lines marked by the right triangle \triangleright and down triangle ∇ signs) nearly identical results are seen and a negligible numerical diffusion is introduced compared to the one introduced by Minmod limiter (lines marked by plus $+$ signs). The Superbee limiter (lines marked by star $*$ signs) gives better results with regards to limiting of the numerical diffusion.

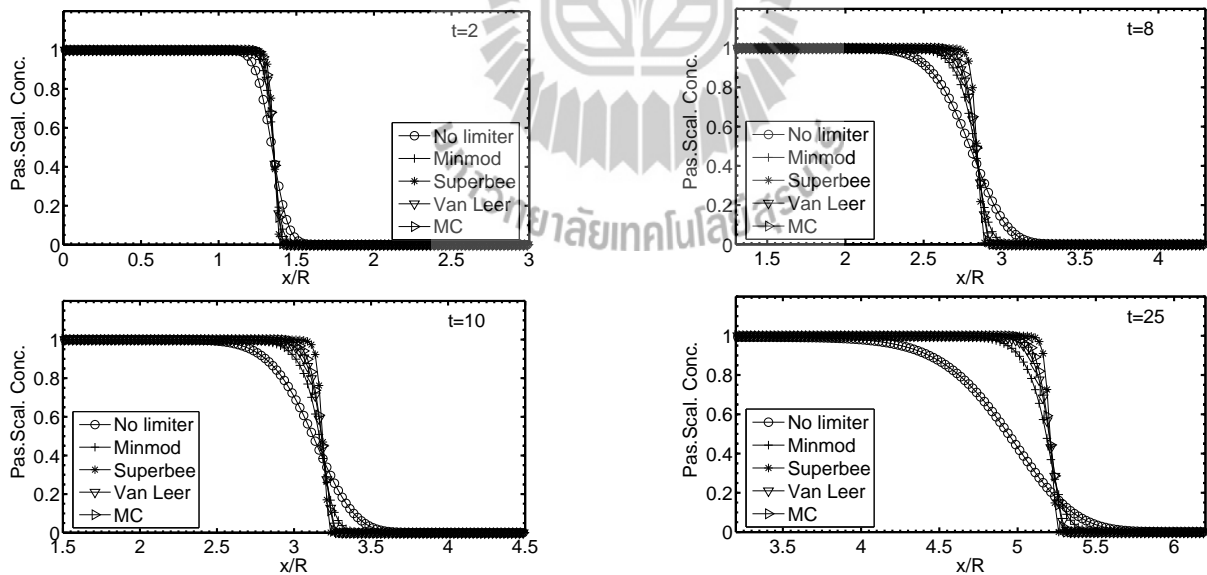


Figure 1.4: Profiles of passive scalar concentrations at transect $z = 0.5\Delta z$ ($C(t, x, 0.5\Delta z)$). Four flux-limiter schemes are compared in the case of $Re = 10^3$, $\Delta x = \Delta z = 0.05$, $\Delta t = 0.001$, \circ – no limiter (first order monotone scheme), $+$ – Minmod, $*$ – Superbee, ∇ – van Leer, \triangleright – MC.

Figures 1.5 shows the graphs of $C(t, x, 0.5\Delta z)$ for different instances of time. Here we compare the four schemes - the Superbee flux-limiter, the SMIF, the ENO3 and the WENO5. For time interval up to $t \simeq 4$ there is almost no difference in performance. For larger times $t \gtrsim 6$ the Superbee limiter gives the smallest numerical diffusion compared

with SMIF, ENO3 and WENO5. Performance of ENO3 and SMIF are nearly identical as seen from data on Figure 1.5 up to time $t \approx 10$. Scheme WENO5 produces less numerical diffusion compared with ENO3 and SMIF.

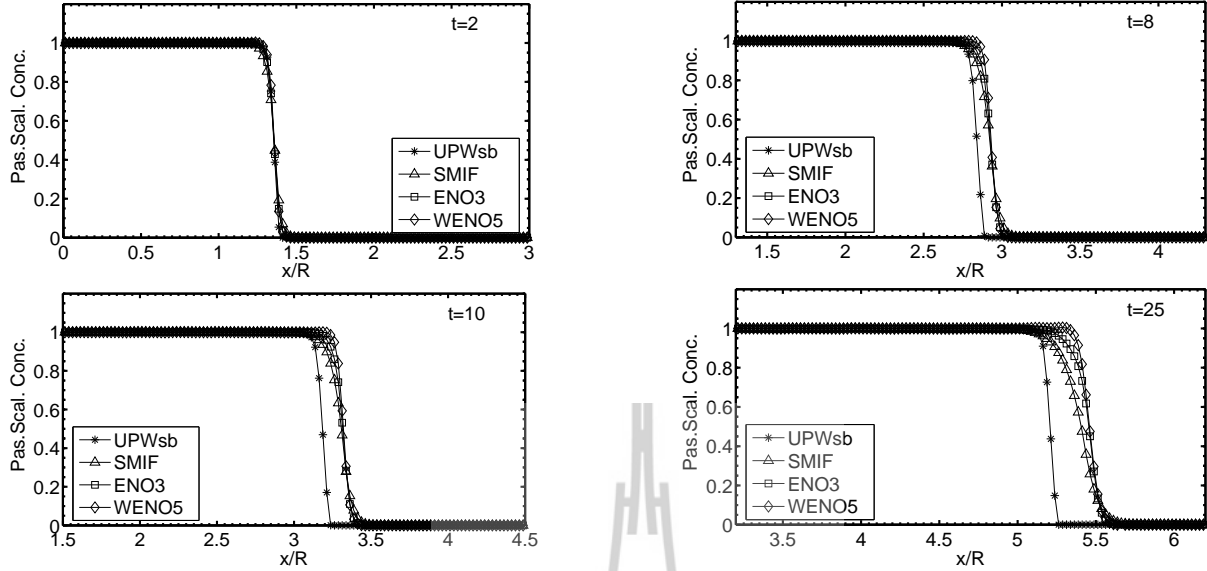


Figure 1.5: Profiles of passive scalar concentrations at transect $z = 0.5\Delta z$ ($C(t, x, 0.5\Delta z)$). Four approximations of convective terms are compared in the case of $Re = 10^3$, $\Delta x = \Delta z = 0.05$, $\Delta t = 0.001$, * - flux-limiter Superbee (UPWsb), Δ - SMIF, \square - ENO3, \diamond - WENO5.

Figure 1.6 illustrates the temporal history of the mixed region width for the four calculations using flux-limiter Superbee (UPWsb) Figure 1.6 a), SMIF Figure 1.6 b), ENO3 Figure 1.6 c), and WENO5 Figure 1.6 d). The stars and triangles are the results of the numerical simulations computed herein. The star signs represent the position $C(t, x^*, 0.5\Delta z) = 0.01$ of passive scalar concentration and the triangle signs represent the position $C(t, x^\blacktriangle, 0.5\Delta z) = 0.99$. The dashed line is drawn according to Wu's [48] original experimental data. The solid curve is made up of two functions:

$$\begin{aligned} x/R &= 1 + 0.29(t/T)^{1.08} \quad \text{for } 0 \leq t/T \leq 2.75, \\ x/R &= 1.03(t/T)^{0.55} \quad \text{for } 2.75 \leq t/T \leq 25, \end{aligned} \tag{1.26}$$

which were found by Wu to fit his experimental data. Figure 1.6 is drawn for $Re = 10^3$, $\Delta x = \Delta z = 0.05$, time increment was $\Delta t = 0.001$. Our numerical results match Wu's experimental data reasonably well (dashed curve in Figures 1.6). The data in Figure 1.6 show that the upwind scheme with Superbee limiter (UPWsb) gives a width of the mixed region which is smaller than Wu's experimental data, but at the same time this scheme has smallest numerical diffusion and as a result numerical smearing of the discontinuity of the concentration of passive scalar ($x^* - x^\blacktriangle$) is smallest. The ENO3 and SMIF schemes reproduced the width of the mixed region nearly identically. The WENO5 scheme gives results closer to Wu's experimental data. Figures 1.7 - 1.10 show Lagrangian particle distributions and contours of the passive scalar concentration at different time instants for the case of $Re = 5 \times 10^4$. Computations were performed on the grid 360×160 with $\Delta x = \Delta z = 0.05$. The time step was $\Delta t = 0.001$. There were 8,050 particles in the mixed region at the initial instant. The shaded domain represents the shape of the mixed region defined by the Lagrangian particles. To make this region transparent we have not drawn all the particles. The solid lines in Figures 1.7 - 1.10 show the evolution

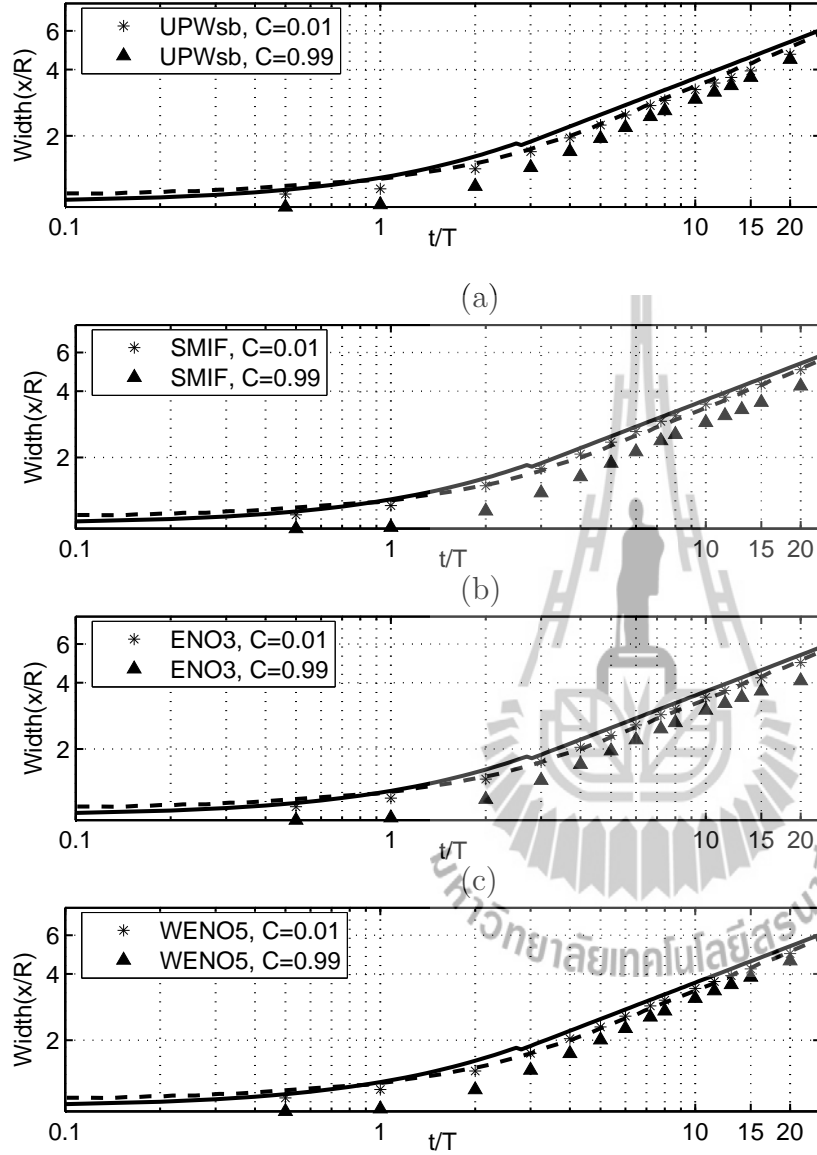


Figure 1.6: Comparisons with Wu's^(d) data $Re = 10^3, \Delta x = \Delta z = 0.05, \Delta t = 0.001$. Flux-limiter Superbee (UPWsb) - (a); SMIF - (b); ENO3 - (c); WENO5 - (d); * corresponds to $C(t, x^*, 0.5\Delta z)$; \blacktriangle corresponds to $C(t, x^\blacktriangle, 0.5\Delta z)$; solid lines represent formulae (1.26), dashed - Wu's experimental data [48].

of the curve $C(t, x, z) = \text{const}$. Lines with letter “a” represent level $C(t, x, z) = 0.01$, lines with letter “b” represent level $C(t, x, z) = 0.5$ and lines with letter “c” represent $C(t, x, z) = 0.99$. In Figure 1.7, we compare the results of five schemes; the first order upwind and the four schemes with flux limiters given by equation (1.22) at time $t = 4$. It can be seen that the Superbee limiter scheme has the smallest dispersion of the passive scalar concentration. If the shape of the mixed region is defined by the contour line $C(t, x, z) = \text{const}$. then the contour level $C(t, x, z) = 0.5$ coincides with shape of a mixed region defined by the Lagrangian particles. Contour lines $C(t, x, z) = 0.01$ define a large domain of the mixed region compared with the region defined by the Lagrangian particles. Contour lines, $C(t, x, z) = 0.99$, are located inside the shaded region for every time instant presented in Figures 1.7 - 1.10. Cross signs (\times) on the x -axis correspond to the width of the mixed region according to Wu’s experiments. It can be seen that contour lines $C(t, x, z) = 0.01$ define the width of the mixed region corresponding to the experimental data. The width of the mixed region defined by a tracer particle for all schemes is smaller than the experimental results of Wu.

In Figure 1.8, we compare the results of four schemes, namely the scheme with Superbee flux-limiter, two adaptive stencil schemes (SMIF and ENO3), and a weighted stencil scheme (WENO5) at time $t = 4$. Performance of the adaptive stencil schemes and weighted stencil scheme are almost identical. We can see that the curve $C(t, x, z) = 0.5$ coincides with the edge of the shaded region. The scheme with Superbee limiter demonstrates a smaller value of the mixed region width compared with SMIF, ENO3 and WENO5.

Figures 1.9 and 1.10 show results of comparison of the four schemes (Superbee, SMIF, ENO3 and WENO5) at the time instants $t = 10, 20$. The qualitative behaviour is similar to the previous case corresponding to $t = 4$. Curve $C(t, x, z) = 0.5$ corresponds to the edge of the shadowed domain. The width of the mixed region defined by Lagrangian particles is smaller than Wu’s experimental results.

Comparison of results for $Re = 10^3$ and $Re = 5 \times 10^4$ demonstrate a weak dependence on the Reynolds number. It was pointed out by [48] that the collapse during the initial ($t \approx 3$) and principal stages ($3 < t < 25$) is primarily a gravitational flow phenomenon, and that the collapse process during these stages is almost identical for different Reynolds numbers. Note that in case of $Re = 10^3$ the computational domain was $10R \times 4R$ in x and z directions, respectively. In case of $Re = 5 \times 10^4$ the computational domain was approximately twice larger, $18R \times 8R$, in the x and z directions, respectively. This note demonstrates that the size of computational domain $10R \times 4R$ is sufficient to shift boundary conditions from infinity to the boundary of the computational domain.

1.5.2 Internal wave generated by collapsing region

The experiments of [48] represent the pattern of internal waves generated by the collapse of the mixed region in the stratified fluid.

The results presented in this section correspond to $Re = 5 \times 10^4$, which is the same as in Wu’s experiment. The total computational domain size, compared to the radius of the initial mixed region, is 18 radii wide and 8 radii high. We used a uniform mesh with grid spacings $\Delta x = \Delta z = 0.05$. Figure 1.11 shows constant density lines at successive time instants. Figure 1.11 shows in detail the collapse of the original mixed region and the growth and propagation of internal waves. During the initial collapse of the mixed region, $t \leq 4$, the fluid layers near the axis $x = 0$ displace towards the center of mixed region ($x = 0, z = 0$) and reach their maximum deflection at the end of the initial collapse stage.

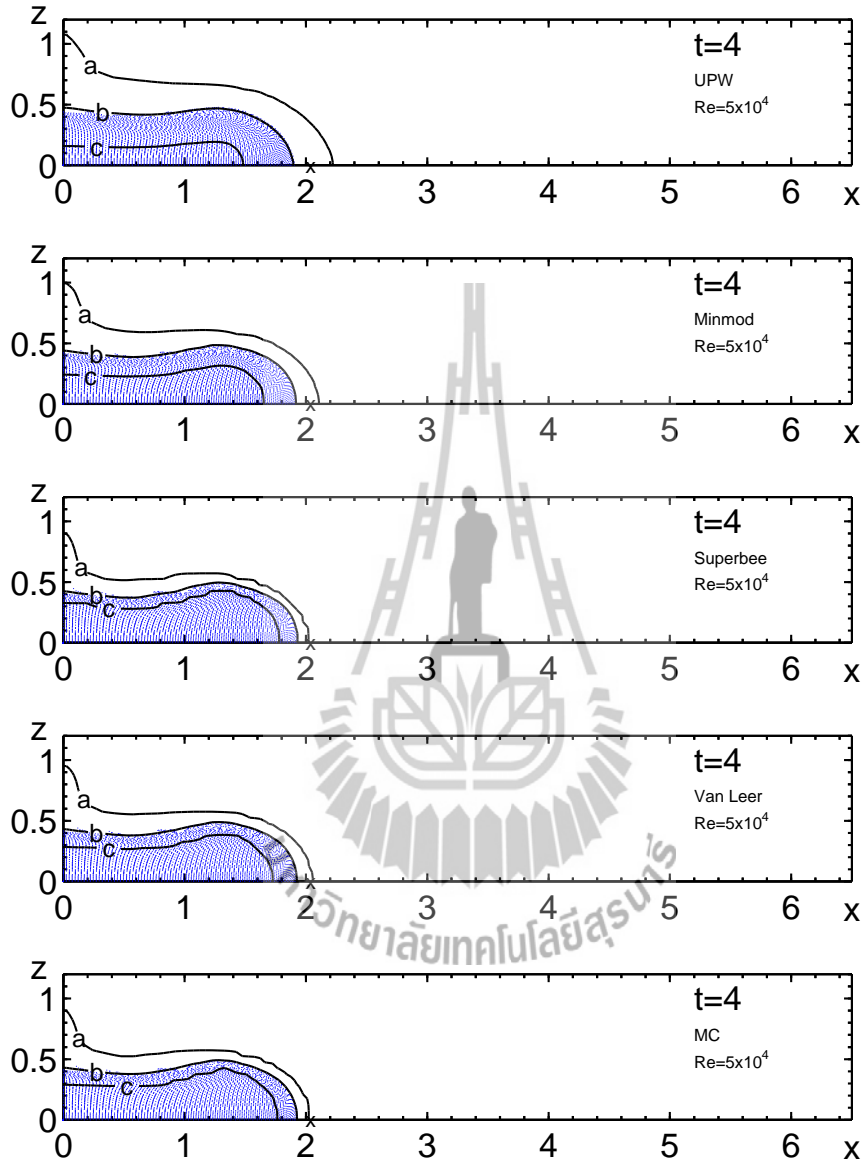


Figure 1.7: Shapes of the collapsed mixed region at time $t = 4$ of 1st-order UPW and four flux-limiters, solid lines represent contour lines from numerical results of passive scalar concentration, shaded areas represent mixed region taken from Lagrangian particles. $Re = 5 \times 10^4$, $\Delta x = \Delta z = 0.05$ and $\Delta t = 0.001$.

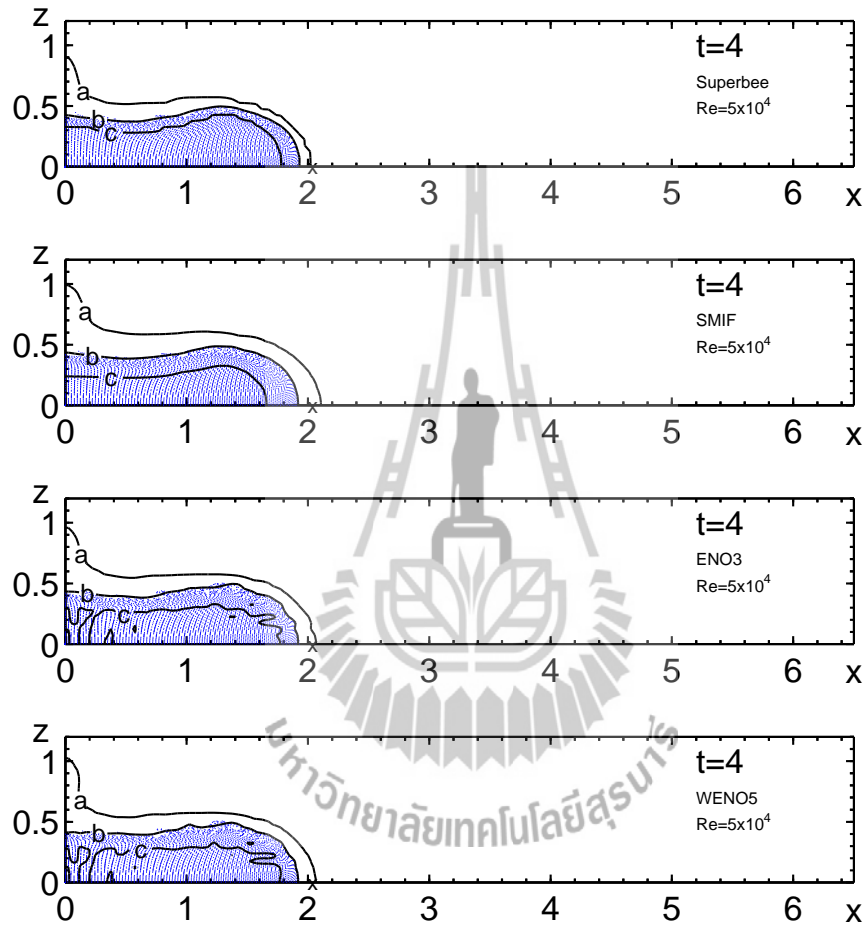


Figure 1.8: Shapes of the collapsed mixed region at time $t = 4$ of Superbee, SMIF, ENO3 and WENO5, solid lines represent contours line from numerical results of passive scalar concentration, shaded areas represent mixed region taken from Lagrangian particles. $Re = 5 \times 10^4$, $\Delta x = \Delta z = 0.05$ and $\Delta t = 0.001$.

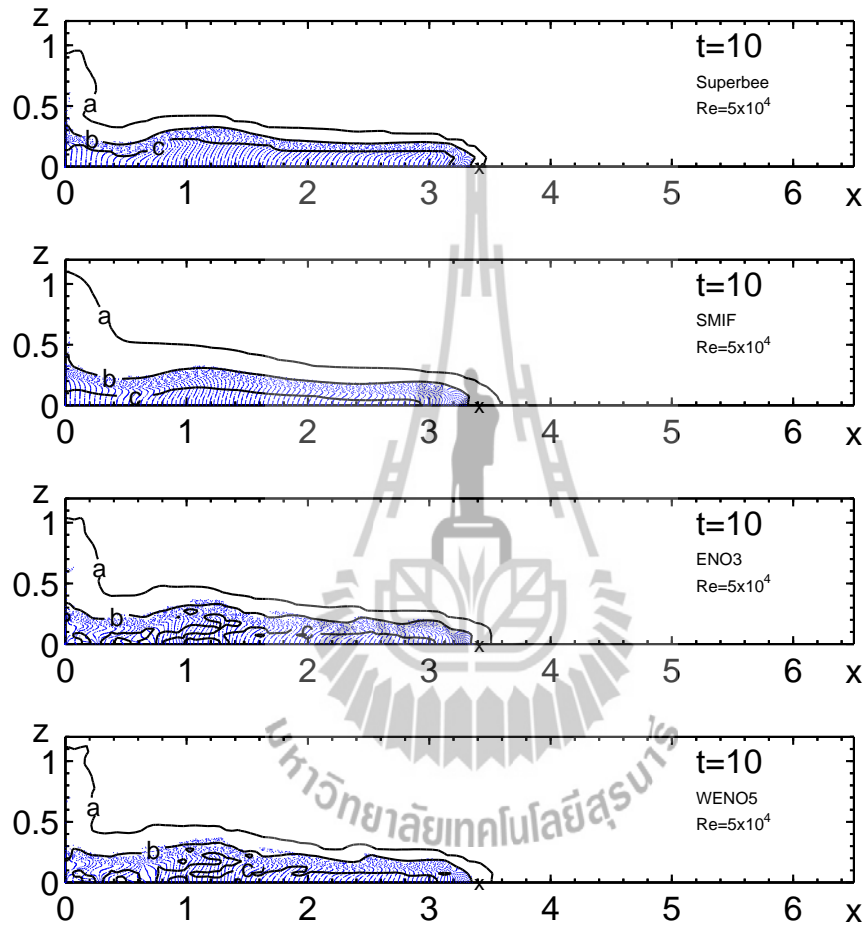


Figure 1.9: Shapes of the collapsed mixed region at time $t = 10$ of Flux-limiter/Superbee, SMIF, ENO3 and WENO5, solid lines represent contour lines from numerical results of passive scalar concentration, shaded areas represent mixed region taken from Lagrangian particles. $Re = 5 \times 10^4$, $\Delta x = \Delta z = 0.05$ and $\Delta t = 0.001$.

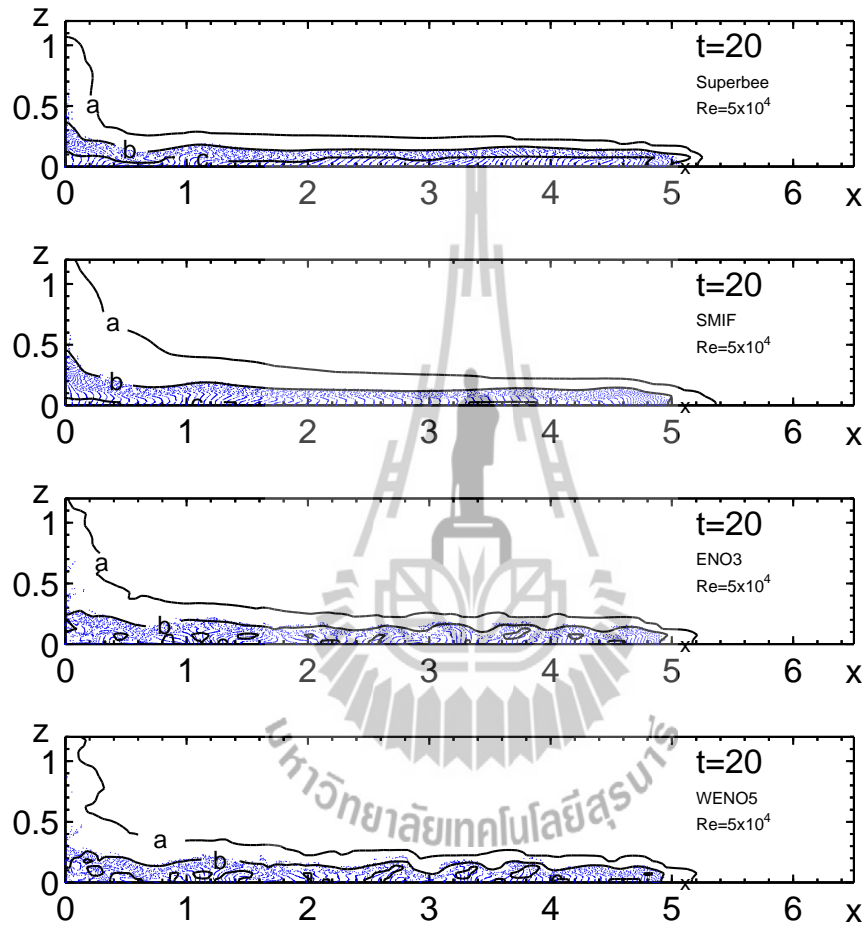


Figure 1.10: Shapes of the collapsed mixed region at time $t = 20$ of Flux-limiter/Superbee, SMIF, ENO3 and WENO5, solid lines represent contour lines from numerical results of passive scalar concentration, shaded areas represent mixed region taken from Lagrangian particles. $Re = 5 \times 10^4$, $\Delta x = \Delta z = 0.05$, and $\Delta t = 0.001$.

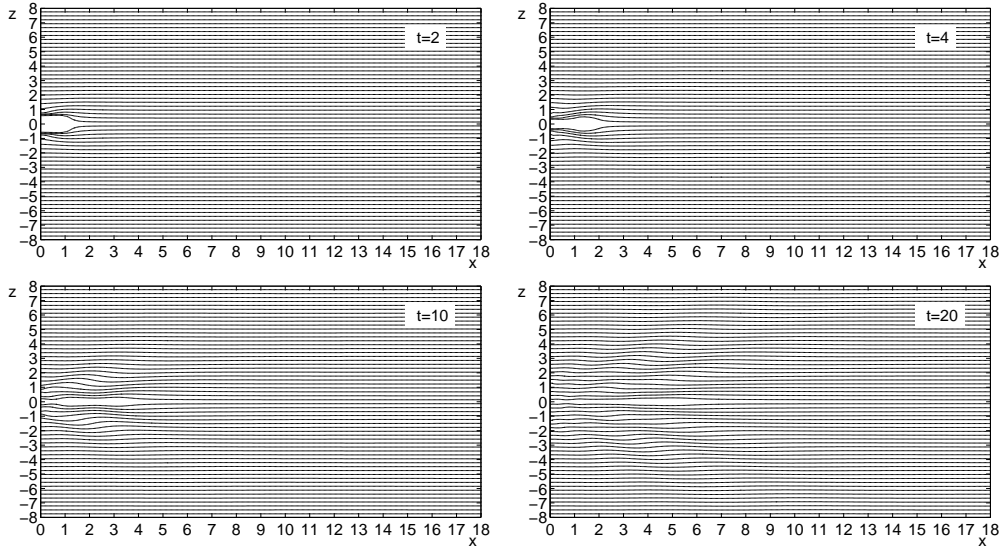


Figure 1.11: The constant density lines, $\rho(t, x, z) = const$, at successive time intervals. Results from SMIF approximation of convective terms are presented for $Re = 5 \times 10^4$, $\Delta x = \Delta z = 0.05$, $\Delta t = 0.001$.

As the deflected layers oscillate back toward their equilibrium positions, undulations of the isopycnic lines are observed.

In order to better understand the wave generated by a collapsing region, the phase pattern of internal waves is illustrated by Figure 1.12, where isolines $\partial\rho_1/\partial x = const$ are drawn at time instants $t = 2, 4, 10,$ and 20 . Lines $\partial\rho_1/\partial x = 0$ correspond to peaks and troughs of internal waves. Not far from the center, except for the small region where the finite size of mixed region is dominant, these lines are almost straight. This agrees with the experimental data of [48]. However, for large distance from the center, the lines $\partial\rho_1/\partial x = 0$ change to a curve. This behaviour of phase lines $\partial\rho_1/\partial x = 0$ does not relate to the method of approximation of convective terms. Other approximations of convective terms used in this work demonstrate similar effects.

1.6 Conclusions and future works

Numerical simulations of the collapse of a fully mixed region in a linearly stratified fluid were considered. The simulations are based on the incompressible Navier-Stokes equations in the Oberbeck-Boussinesq approximation. Three groups of high-order monotone finite difference schemes have been successfully tested and compared within this problem.

1. The flux-limiter schemes used a 'fixed' stencil and demonstrated reasonable accuracy and had small numerical diffusion. The Superbee limiter had smallest smearing of discontinuity, is not recommended for the problem considered because it significantly reduces the convection velocity of discontinuity.
2. Two schemes with 'adaptive' stencil are ENO3 and SMIF. They obey small numerical diffusion and results obtained using these schemes are in good agreement with experimental data.
3. The WENO5 scheme is a 'weighted' stencil method. The WENO5 does better reproduce experimental data compared with the other methods used in this paper.

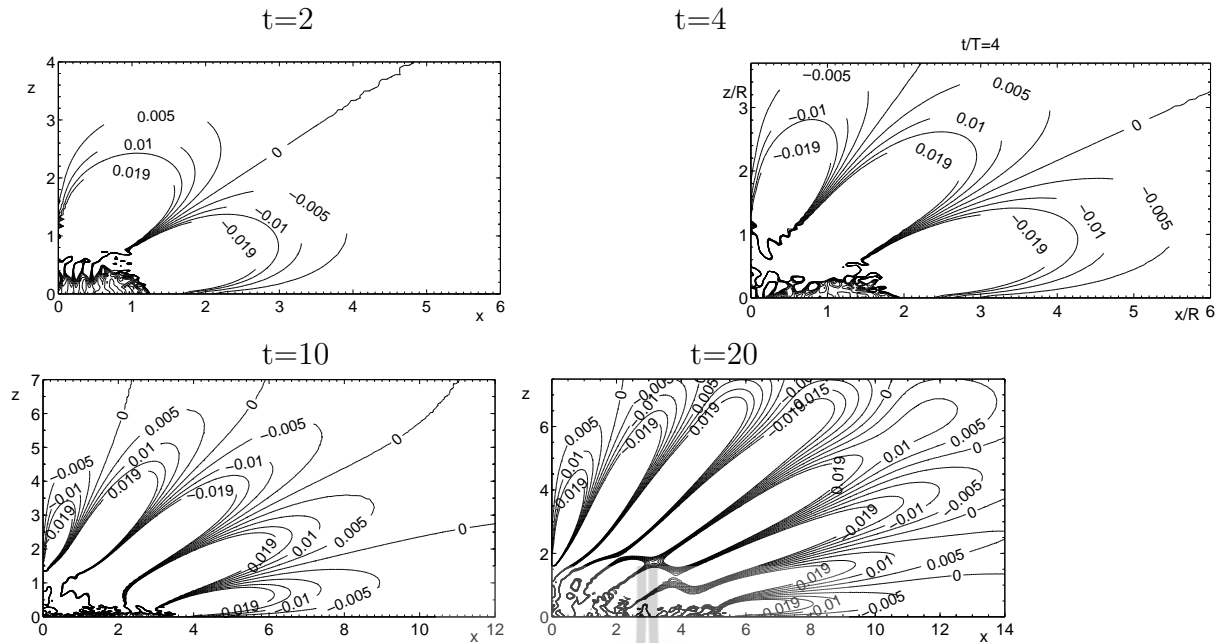


Figure 1.12: Isolines $\partial\rho_1/\partial x = const.$ Computational results from WENO5 approximation of convective terms with $Re = 5 \times 10^4$, $\Delta x = \Delta z = 0.05$ and $\Delta t = 0.001$.

Because the WENO5 scheme used a stencil which contains discontinuity we observed small dispersion in the area of discontinuity.

From the results of numerous computational tests, some recommendations can be made. To reproduce the initial stage of collapse of the mixed region all considered schemes gave sufficiently accurate results. For large time of collapse, SMIF, ENO3 or WENO5 scheme have to be used.

A more significant influence of different high-order upwind approximations on the pattern of the internal waves is observed for waves with density level corresponding to the density of unperturbed fluid on the levels of the mixed region.

The work done in this report is the very beginning stage of a project whose ultimate goal is the development of a numerical model applicable to the realistic geophysical flows in natural environment. Planned work includes extension of numerical model to flows in media with nonlinear stratification and to a large time of degeneration corresponding the final stage of collapse.

1.7 Acknowledgements

The research was supported by Suranaree University of Technology and by the Office of the Higher Education Commission under the NRU project.

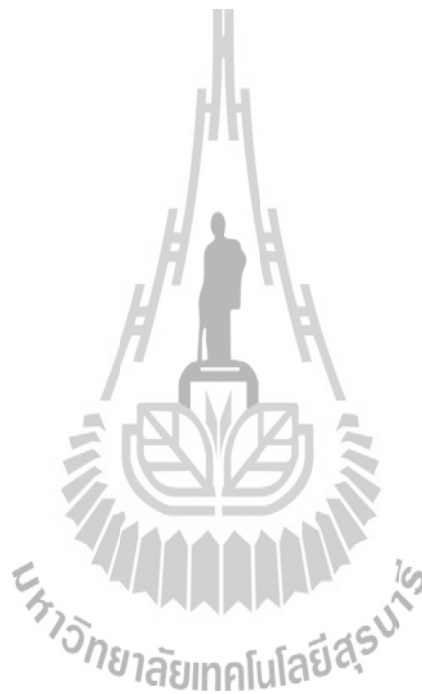
Bibliography

- [1] K. N. Fedorov, *Fine Thermohaline Structure of Oceanic Water*, Gidrometeoizdat, Leningrad, (1976), 183 pages (in Russian).
- [2] A. S. Monin and R. V. Ozmidov, *Oceanic Turbulence*, Gidrometeoizdat, Leningrad, (1981), (in Russian).
- [3] J. M. Lighthill, *Waves in Fluids*, Cambridge University Press, ed. 2, England, (2002), 520 pages.
- [4] J. R. Munroe, C. Voegel, B. R. Sutherland, V. Birman, E. H. Meiburg, Intrusive gravity currents from finite-length locks in a uniformly stratified fluid, *Journal of Fluid Mechanics*, vol. 635, (2009), p. 245–273.
- [5] A.A. Amsden, F.H. Harlow, The SMAG method, Los Alamos Scient. Lab. Rept., LA-4370, (1970).
- [6] A.V. Babakov, Application of flow theory to a problem of the dynamics of a viscous stratified fluid, *USSR Comput Math. Math. Phys.*, vol. 23, Iss. 2, (1983) 115–119.
- [7] O.M. Belotserkovskii, *Mathematical modelling in Informatics: Numerical Simulation in the Mechanics of Continuous Media*, Moscow, Russia, (1997).
- [8] O. F. Voropaeva and G. G. Chernykh, Internal waves generated by momentumless turbulent wake in a linearly stratified fluid, *Mathematical Modeling*, vol. 10, No. 6, (1998), p. 75–89.
- [9] O. F. Voropaeva, N. P. Moshkin and G. G. Chernykh, Internal waves generated by turbulent wakes in a stably stratified medium *Doklady Physics*, vol. 48, no. 9, (2003), p. 517–521.
- [10] N. P. Moshkin, G. G. Chernykh and A. V. Fomina, On the influence of small total momentum imbalance on turbulent wake dynamics in the linearly stratified medium, *Mathematical Modeling*, vol. 17, no. 1, (2005), p. 19–33.
- [11] J. Wu, Mixed region collapse with internal wave generation in a density-stratified medium, *Journal of Fluid Mechanics*, vol. 35, (1969), p. 531–544.
- [12] W. R. Wessel, Numerical study of the collapse of a perturbation in an infinite density stratified fluid, *Physics of Fluids*, vol. 12, no. 12, (1969), p. 170–176.
- [13] Yu. M. Lytkin and G. G. Chernykh, On internal waves induced by the mixing zone collapse in a stratified fluid, *Mathematical Problems of Mechanics (Continuum Dynamics)*, Institute of Hydrodynamics, Sib. Branch USSR Akad. Sci., Novosibirsk, vol. 22, (1975), p. 116–132.

- [14] V. P. Nartov and G. G. Chernykh, On numerical modeling of fluid flow generated by collapse of mixed region in stratified medium, Institute of Theoretical and Applied Mechanics, Novosibirsk, (1982), Preprint (in Russian).
- [15] E. V. Vorozhtsov and N. N. Yanenko, Methods for the Localization of Singularities in Numerical Solutions of Gas Dynamics Problems, Springer-Verlag, New York, 1989.
- [16] C. Hirsch, Numerical Computational of Internal and External Flows, Vol. 2: Computational Methods for Inviscid and Viscous Flows, John Wiley and Sons, 1991.
- [17] T. J. Chung, Computational Fluid Dynamics, Cambridge University Press, 2002.
- [18] J. P. Boris and D. L. Book, Flux-corrected transport. III. minimal-error FCT algorithms, Journal of Computational Physics, vol. 20, no. 4, (1976), p. 397–431.
- [19] D. Brown, R. Cortez, M.I. Minion, Accurate projection methods for the incompressible Navier-Stokes equations, J. Comput. Phys., vol. 168, (2001) 464–499.
- [20] G.G. Chernykh, O.F. Voropaeva, On numerical modelling of local density perturbation dynamics using moving grids, J. Eng. Thermophysics, vol. 20, No. 3, (2011) 290–301.
- [21] S.K. Godunov, A Difference Scheme for Numerical Solution of Discontinuous Solution of Hydrodynamic Equations, Math. Sbornik, vol. 47, (1959) 271–306, (translated US Joint Publ. Res. Service, JPRS 7226, 1969).
- [22] K.N. Fedorov, Fine Thermohaline Structure of Oceanic Water, Gidrometeoizdat, Leningrad, (1976) (in Russian).
- [23] M. Fortin, R. Peyret, R. Temam, Résolutions numériques des équations de Navier-Stokes pour un fluide incompressible, J.de Mécanique, vol. 3, No. 10, (1971) 357–390.
- [24] H. E. Gilreath, A. Brandt, Experiments on the generation of internal waves in a stratified fluid, AIAA J., vol. 23, (1985) 693–700.
- [25] V.A. Gushchin, The splitting method for problems of the dynamics of an inhomogeneous viscous incompressible fluid, USSR Comput. Math. Math. Phys., vol. 21, Iss. 4, (1981) 190–204.
- [26] V.A. Gushchin, V.N. Konshin, Computational aspects of the splitting method for incompressible flow with a free surface, Comp. Fluids, vol. 21, (1992) 345–353.
- [27] V.A. Gushchin, P.V. Matyushin, Numerical simulation of separated flow past a sphere, Comput. Math. Math. Phys., vol. 37, (1997) 1086–1100.
- [28] A. Harten, High-resolution schemes for hyperbolic conservation laws, J. Comput. Phys., vol. 49, (1983) 357–393.
- [29] A. Harten, B. Engquist, S. Osher, S. Chakravarthy, Uniformly high order accurate essentially non-oscillatory schemes, III, J. Comput. Phys., vol. 71, (1987) 231–303.
- [30] R.J. LeVeque, High-resolution conservative algorithms for advection in incompressible flow, SIAM J. Numer. Anal., vol. 33, (1996) 627–665.
- [31] J. Lighthill, Waves In Fluids, Cambridge University Press, 2nd edition, (2002).

- [32] Yu.M. Lytkin, G.G. Chernykh, On internal waves induced by the mixing zone collapse in a stratified fluid, In: *Mathematical Problems of Mechanics (Continuum Dynamics)*, vol. 22, Inst. of Hydrodynamics, Sib. Branch USSR Akad. Sci., Novosibirsk, (1975) 116-132 (in Russian).
- [33] V.S. Maderich, V.I. Nikishov, A.G. Stetsenko, *Internal Mixing Dynamics in a Stratified Medium*, Naukova Dumka, Kiev, (1988) (in Russian).
- [34] A.S. Monin, R.V. Ozmidov, *Oceanic Turbulence*, Gidrometeoizdat, Leningrad, (1981) (in Russian).
- [35] N.P. Moshkin, G.G. Chernykh, A.V. Fomina, On the influence of small total momentum imbalance on turbulent wake dynamics in the linearly stratified medium, *Matem. Model.*, vol. 17, No. 1, (2005) 19–33.
- [36] J.R. Munroe, C. Voegeli, B.R. Sutherland, V. Birman, E.H. Meiburg, Intrusive gravity currents from finite-length locks in a uniformly stratified fluid, *J. Fluid Mech.*, vol. 635, (2009) 245–273.
- [37] V.P. Nartov, G.G. Chernykh, On numerical modelling of fluid flow generated by collapse of mixed region in stratified medium, Preprint, Institute of Theoretical and Applied Mechanics, Novosibirsk, (1982) (In Russian).
- [38] B. Roe, Some contributions to the modeling of discontinuous flows, *Lect. Notes Appl. Math.*, 1985, vol. 22, pp. 163–193.
- [39] B. Roe, D. Sidilkover, Optimum positive linear schemes for advection in two and three dimensions, *SIAM J. Num. Anal.*, vol. 29, (1992) 1542–1568.
- [40] C.-W. Shu, Essentially non-oscillatory and weighted essentially nonoscillatory schemes for hyperbolic conservation laws. *Advanced Numerical Approximation of Nonlinear Hyperbolic Equations*; Quarteroni, A., Ed.; Springer-Verlag: Berlin, vol. 1697, (1998) 325–432.
- [41] J.S. Turner, *Buoyancy Effects in Fluids*. Cambridge University Press, Cambridge, (1973).
- [42] B. Van Leer, Towards the ULTIMATE conservation difference scheme. II. Monotonicity and conservation combined in a second order scheme, *J. Comput. Phys.*, vol. 14, (1974) 361–370.
- [43] B. Van Leer, Towards the ULTIMATE conservation difference scheme. IV. A new approach to numerical convection, *J. Comput. Phys.*, vol. 23, (1977) 276–299.
- [44] O.F. Voropaeva, G.G. Chernykh, Internal waves generated by momentumless turbulent wake in a linearly stratified fluid, *Matem. Model.*, vol. 10, No. 6, (1998) 75–89.
- [45] O.F. Voropaeva, N.P. Moshkin, G.G. Chernykh, Internal waves generated by turbulent wakes in a stably stratified medium, *Dokl. Phys.*, vol. 48, No. 9, (2003) 517–521.
- [46] E.V. Vorozhtsov, N.N. Yanenko, *Methods for the localization of singularities in numerical solutions of gas dynamics problems*, Springer-Verlag, New York, (1989).

- [47] W. R. Wessel, Numerical study of the collapse of a perturbation in an infinite density-stratified fluid, *Phys. Fluids*, vol. 12, No. 12, pt.II, (1969) 170–176.
- [48] J. Wu, Mixed region collapse with internal wave generation in a density-stratified medium, *J. Fluid. Mech.*, vol. 35, pt. 3, (1969) 531–544.
- [49] N.N. Yanenko, *The Method of Fractional Steps. The Solution of Problems of Mathematical Physics in Several Variables*, New York: Springer, (1971).
- [50] R. Zhang, M. Zhang, C.-W. Shu, On the order of accuracy and numerical performance of two classes of finite volume WENO schemes, *Commun. Comput. Phys.*, vol. 9, (2011) 807–827.

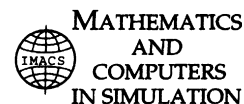




Available online at www.sciencedirect.com

SciVerse ScienceDirect

Mathematics and Computers in Simulation xxx (2013) xxx–xxx



www.elsevier.com/locate/matcom

Original article

On the performance of high resolution non-oscillating advection schemes in the context of the flow generated by a mixed region in a stratified fluid

N.P. Moshkin^{a,*}, G.G. Chernykh^b, Kridsada Narong^c

^a *Institute of Science, School of Mathematics, Suranaree University of Technology, Nakhon Ratchasima, Thailand*

^b *Institute of Computational Technologies, SB RAS, Novosibirsk 630090, Russia*

^c *Department of Mathematics, Statistics and Computer, Ubon Ratchathani University, Ubon Ratchathani 34190, Thailand*

Received 25 October 2011; received in revised form 30 July 2012; accepted 23 November 2012

Abstract

The two-dimensional flow generated by a local density perturbation (fully mixed region) in stratified fluid is considered. In order to describe accurately the sharp discontinuity in density at the edge of the mixed region, monotone schemes of high order of approximation are required. Although a great variety of methods have been developed during the last decades, there remains the question of which method is the best. This present paper deals with the numerical treatment of the advective terms in the Navier–Stokes equations in the Oberbeck–Boussinesq approximation. Comparisons are made between the upwind scheme, flux-limiter schemes, namely Minmod, Superbee, van Leer and monotone centred (MC), monotone adaptive stencil schemes, namely ENO3 and SMIF, and the weighted stencil scheme WENO5. We used the laboratory experimental data of Wu as a benchmark test to compare the performance of the various numerical approaches. We found that the flux limiter schemes have the smallest numerical diffusion. On the other hand, the WENO5 scheme describes the variation of the width of the collapsing region over time most accurately. All considered schemes give realistic patterns of internal gravity waves generated by the collapsing region.

© 2012 IMACS. Published by Elsevier B.V. All rights reserved.

Keywords: Collapse of mixed region; Stratified fluid; High order non-oscillating scheme

1. Introduction

The problem of a two-dimensional fully mixed region collapsing in a continuously density-stratified medium is considered. The interest in this problem stems from the study of a number of geophysical phenomena and a number of technical problems [7,16,18,19,26,21]. For example, because the turbulent wake behind a body traveling through stratified fluid is very slender in the direction of body motion, the flow field and internal waves induced by the wake can be adequately described by studying the collapse of a non-turbulent mixed region in stratified medium [9,16,20,29,30]. There are numerous studies focusing on locally homogeneous perturbations of the density field (fully mixed region). Experimental work on this problem has been done by Wu [33]. To the best of the authors' knowledge, Wessel [32] was the first who solved the Navier–Stokes equations in the Oberbeck–Boussinesq approximation numerically for the case

* Corresponding author. Tel.: +66 44 22 46 25; fax: +66 44 22 41 85
E-mail address: nikolay.moshkin@gmail.com (N.P. Moshkin).

of sharp discontinuity in density at the mixed region edge. He obtained general corroboration with the experiment of Wu [33] in terms of wave patterns and the horizontal size of the mixed region for large time instants. The properties of the internal wave patterns are well described in Lytkin and Chernykh [17] for the laminar collapse of a mixed region having various initial density perturbations in a linearly stratified medium. This problem was used by several researchers as a benchmark test in order to assess the performance of some numerical algorithms which they constructed [2,10]. In Nartov and Chernykh [22] to study the history of the shape of the mixed region, the idea of a non-diffusing passive scalar was used. The method for the localization of singularities [31] was utilized to define the location of the edge of the mixed region. A more complete list of references and more comprehensive overview of research can be found in Chernykh and Voropaeva [5].

Incompressible viscous flow at variable density presents the difficulty of satisfying the property of mass conservation in two respects. On the one hand, the mass density of each fluid particle must remain unchanged during the fluid motion, whatever the level of unsteadiness and mixing. On the other hand, the velocity field must satisfy the incompressibility constraint which reflects the inability of pressure to do compression work. To describe the sharp discontinuity in density at the mixed region edge with sufficient accuracy, schemes of high order of approximation are required. Godunov's theorem [6] states that any linear monotonic advection schemes cannot provide better than first-order accuracy. Therefore, there is a need to apply higher order accuracy numerical schemes derived for numerical solutions of conservation laws which support discontinuous solutions. Many methods match additional requirements, for example; they are Lax–Wendroff, Lax–Friedrichs, flux corrected transport (FCT) methods of Boris–Book and Zalesak, slope limiter methods of van Leer, essentially non-oscillatory (ENO) schemes of Harten–Shu–Osher and total variation diminishing schemes (TVD). Even though there are very little theoretical results about the properties of such schemes in multidimensional and nonlinear cases, in practice these schemes are very robust and stable, and they are used in a lot of practical applications. Yet, there is always the question of what is the best choice, the answer to which is obviously problem dependent. In this research several high order resolution advection schemes will be used to solve the problem of mixed region dynamics in a stratified fluid. A comparative analysis of the effectiveness of the advection schemes will be obtained.

2. Mathematical formulation

The governing equations are the Navier–Stokes equations in the Oberbeck–Boussinesq approximation:

$$\frac{\partial u}{\partial t} + u \frac{\partial u}{\partial x} + w \frac{\partial u}{\partial z} + \frac{1}{\rho_0} \frac{\partial p_1}{\partial x} = \nu \left(\frac{\partial^2 u}{\partial x^2} + \frac{\partial^2 u}{\partial z^2} \right), \quad (1)$$

$$\frac{\partial w}{\partial t} + u \frac{\partial w}{\partial x} + w \frac{\partial w}{\partial z} + \frac{1}{\rho_0} \frac{\partial p_1}{\partial z} = \nu \left(\frac{\partial^2 w}{\partial x^2} + \frac{\partial^2 w}{\partial z^2} \right) - g \frac{\rho_1}{\rho_0}, \quad (2)$$

$$\frac{\partial u}{\partial x} + \frac{\partial w}{\partial z} = 0, \quad (3)$$

$$\frac{\partial \rho}{\partial t} + u \frac{\partial \rho}{\partial x} + w \frac{\partial \rho}{\partial z} = 0. \quad (4)$$

Here ν is the coefficient of kinematic viscosity, u and w are the components of velocity in x and z directions of Cartesian coordinates as shown in Fig. 1, $\rho = \rho(x, z, t)$ is the density, $\rho_1(x, z, t) = \rho(x, z, t) - \rho_s(z)$, $\rho_s = \rho_s(z)$ is the density of undisturbed media, $\rho_0 = \rho_s(0)$, p_1 is the deviation of pressure from hydrostatic pressure, and g is the gravitational acceleration. The stratification is assumed to be linear and stable, i.e., $d\rho_s/dz = -a\rho_0$, where $a = \text{const} > 0$. The boundary and initial conditions are

$$\rho_1 = 0, \quad u = w = 0, \quad \text{if } x^2 + z^2 \rightarrow \infty, \quad t \geq 0, \quad (5)$$

$$\rho = \begin{cases} \rho_0, & \text{if } (x, z) \in A, \quad t = 0, \\ \rho_s(z), & \text{if } (x, z) \notin A, \quad t = 0, \end{cases} \quad (6)$$

$$u = w = 0, \quad \text{if } -\infty < x, z < \infty, \quad t = 0. \quad (7)$$

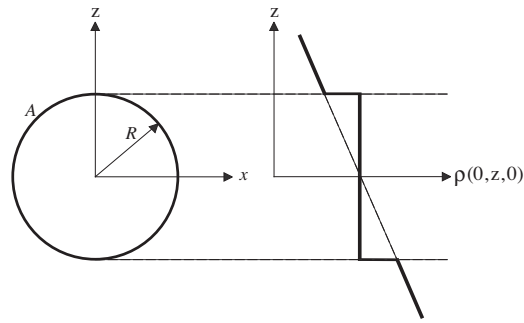


Fig. 1. A circular mixed region with full mixing.

Here A is the domain of totally mixed fluid, in our particular case, $A = \{(x, z) : x^2 + z^2 \leq R^2\}$. System of Eqs. (1)–(4), initial and boundary conditions (5)–(7) can be cast in a dimensionless form by using R as the scale of length (the mixing zone radius), and Vaisala–Brunt period, $T = 1/\sqrt{a_0g}$, as time scale: besides, the representation $\rho = \rho_0 a R \bar{\rho}$ ($\bar{\rho}$ denotes dimensionless density) is used. As a result, the value $1/Re = \nu T/R^2$ appears in the dimensionless equations instead of ν , and 1 instead of g .

To study the history of the shape of the mixed region, the idea of non-diffusing passive scalar will be used. The transport equation of passive scalar is solved together with system (1)–(4):

$$\frac{\partial C}{\partial t} + u \frac{\partial C}{\partial x} + w \frac{\partial C}{\partial z} = 0, \tag{8}$$

with initial and boundary conditions

$$C(0, x, z) = \begin{cases} C_0 = \text{const}, & \text{if } (x, z) \in A, \\ 0, & \text{if } (x, z) \notin A, \end{cases} \quad t = 0, \tag{9}$$

$$C(t, x, z) = 0, \quad \text{if } x^2 + z^2 \rightarrow \infty, \quad t > 0. \tag{10}$$

Here $C(t, x, z)$ is the concentration of the passive scalar. The edge of the mixed region can be defined as the location of the discontinuity in passive scalar concentration. The motion of passive Lagrangian particles is also used to visualize the flow.

3. Numerical scheme

A finite difference scheme is used for the numerical solution of the governing equations. Variables are discretized on a uniform rectangular grid of mesh size Δx and Δz in the horizontal and vertical directions, respectively, and the time step is denoted by Δt . For the sake of simplicity of a numerical algorithm representation, the system of equations is recast in the following form:

$$\mathbf{u}_t + (\mathbf{u} \cdot \nabla) \mathbf{u} = -\nabla p + \frac{1}{Re} \Delta \mathbf{u} - \rho_1 \mathbf{z}, \tag{11}$$

$$\rho_t + (\mathbf{u} \cdot \nabla) \rho = 0, \tag{12}$$

$$\nabla \cdot \mathbf{u} = 0, \tag{13}$$

where ρ is the density, \mathbf{u} is the velocity vector, and \mathbf{z} is the unit vector in direction opposite to the gravitational force. In two-dimensional space the staggered grid as shown in Fig. 2 and the following notations $\mathbf{u} = (u, w)$, $\mathbf{q} = (u, w, \rho) = (\mathbf{u}, \rho)$ are used. The notations in Fig. 2 are described as follows: let Ω_{ij} be the (i, j) th grid cell $[x_{i-1/2}, x_{i+1/2}] \times [z_{j-1/2}, z_{j+1/2}]$, the “edge velocities” $u_{i\pm 1/2, j}$ and $w_{i, j\pm 1/2}$ are the velocity components at the midpoints of the interfaces $(x_{i\pm 1/2},$

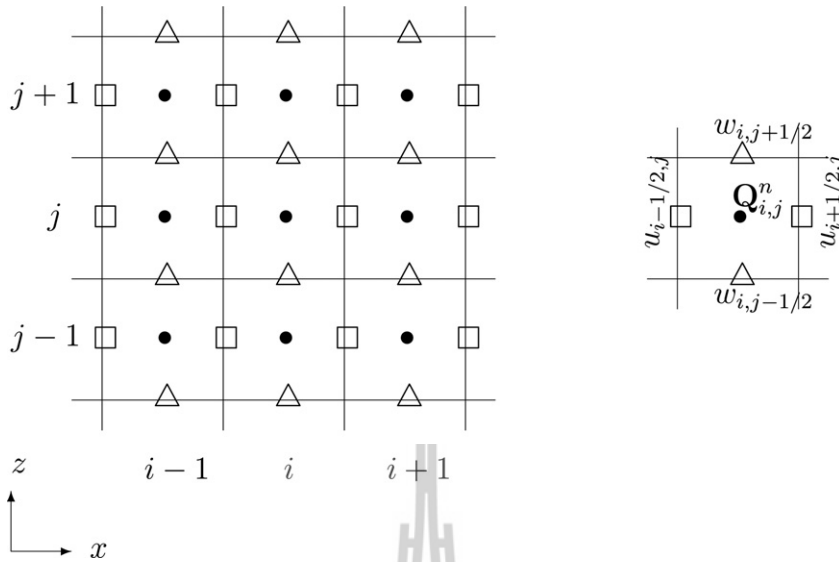


Fig. 2. Staggered grid: (□) u , (Δ) w and (●) Q (or U).

z_j) and $(x_i, z_{j\pm 1/2})$, and the centered values Q_{ij}^n and U_{ij}^n represent an approximation to the cell average of q and u at the current time level $t^n = t^{n-1} + \Delta t$:

$$Q_{ij}^n = \frac{1}{\Delta x \Delta z} \int_{\Omega_{ij}} \mathbf{q}(x, z, t) dx dz, \quad U_{ij}^n = \frac{1}{\Delta x \Delta z} \int_{\Omega_{ij}} \mathbf{u}(x, z, t) dx dz. \tag{14}$$

The projection method for the above system (11)–(13) can be stated as follows:

- *Step I:* Use the centered values $Q^n = (U^n, W^n, \rho^n)$ and edge values $u^n = (u^n, w^n)$ to solve the advection equation

$$\frac{\tilde{Q} - Q^n}{\Delta t} + u^n \cdot \nabla Q^n = 0. \tag{15}$$

This is solved on a finite volume grid using the explicit high-resolution monotone algorithm. The resulting solution is $\tilde{Q} = (\tilde{U}, \tilde{W}, \rho^{n+1}) = (\tilde{U}, \rho^{n+1})$.

- *Step II:* Use a Crank–Nicolson discretizing for diffusion

$$\frac{U^* - \tilde{U}}{\Delta t} = \frac{1}{2Re} (\nabla^2 U^n + \nabla^2 U^*) - \rho_1^{n+1} z. \tag{16}$$

Spacial centered finite differences are used to approximate diffusive terms in above equation. This gives the intermediate velocity $U^* = (U^*, W^*)$ at the cell center.

- *Step III:* Obtain the edge velocity by

$$u^{n+1} = u^* - \mathcal{G}(\Delta t \phi^{n+1}), \tag{17}$$

where the function ϕ denotes the scalar potential in the Hodge decomposition theorem, $u^* = (u^*, w^*)$ is the average of the adjacent U^* ,

$$u_{i-1/2,j}^* = \frac{1}{2}(U_{i-1,j}^* + U_{i,j}^*), \quad w_{i,j-1/2}^* = \frac{1}{2}(W_{i,j-1}^* + W_{i,j}^*),$$

and \mathcal{G} is the discrete gradient operator defined as follows:

$$\mathcal{G}\phi_{i,j} = \left(\frac{\phi_{i,j} - \phi_{i-1,j}}{\Delta x}, \frac{\phi_{i,j} - \phi_{i,j-1}}{\Delta z} \right).$$

The update (17) requires the values ϕ^{n+1} , which can be obtained by solving a discrete Poisson problem $\mathcal{D}\mathcal{G}(\Delta t\phi)_{ij}^{n+1} = (\mathcal{D}\mathbf{u}^*)_{ij}$, where \mathcal{D} is the discrete divergence operator defined as follows:

$$(\mathcal{D}\mathbf{u})_{i,j} = \frac{u_{i+1/2,j} - u_{i-1/2,j}}{\Delta x} + \frac{w_{i,j+1/2} - w_{i,j-1/2}}{\Delta z}.$$

The value ϕ^{n+1} is obtained by the fractional step method with stabilizing correction [34]. The pressure p^{n+1} can be obtained from ϕ^{n+1} through the relationship [4],

$$p^{n+1} = \phi^{n+1} - \frac{\Delta t}{2Re} \nabla^2 \phi^{n+1}.$$

- *Step IV:* In the final step, we update the cell-centered velocity by

$$U_{i,j}^{n+1} = U_{i,j}^* - \frac{\Delta t}{2} \frac{\phi_{i+1,j}^{n+1} - \phi_{i-1,j}^{n+1}}{\Delta x},$$

$$W_{i,j}^{n+1} = W_{i,j}^* - \frac{\Delta t}{2} \frac{\phi_{i,j+1}^{n+1} - \phi_{i,j-1}^{n+1}}{\Delta z}.$$

This completes one time step. Go to Step I for next time step.

3.1. The high resolution numerical methods for transport equations

A monotone scheme of high order of approximation is required to describe the discontinuity in density at the edge of the mixed region with sufficient accuracy. For simplicity, a brief illustration of the algorithms used, we consider the one-dimensional scalar advection equation in a specified incompressible velocity field $u(t, x)$:

$$\frac{\partial Q}{\partial t} + \frac{\partial u Q}{\partial x} = 0, \tag{18}$$

where Q is a conservative quantity which can be a velocity component, density or passive scalar concentration function. The flux of quantity Q is denoted by F . A regular spacial grid is defined by the points $x_i = i\Delta x$, $i=0, 1, \dots, N$ also called the cell centers. The time step is denoted by Δt . To maintain the conservative property of (18) the numerical flux $\widehat{F}(x, t)$ is implicitly defined by

$$F(x, t) = \frac{1}{\Delta x} \int_{x-\Delta x/2}^{x+\Delta x/2} \widehat{F}(x, t) dx,$$

such that the derivative $\partial F/\partial x$ is calculated exactly by the following formula:

$$\frac{\partial F}{\partial x}(x, t) = \frac{\widehat{F}(x + \Delta x/2, t) - \widehat{F}(x - \Delta x/2, t)}{\Delta x}.$$

Hence, discretization of Eq. (18) is obtained in the flux form and can be expressed explicitly in time as

$$Q_i^{n+1} = Q_i^n - \frac{\Delta t}{\Delta x} \left[\widehat{F}_{i+1/2}^n - \widehat{F}_{i-1/2}^n \right], \tag{19}$$

where n is the time level, $t^n = n\Delta t$, $Q_i^n = Q(x_i, t^n)$ and $\widehat{F}_{i\pm 1/2}^n$ are the Q fluxes through the right and left boundaries of the grid cell, respectively. In the sections below, the different numerical approximations of the $\widehat{F}_{i\pm 1/2}^n$ in (19) that are used in this work are presented. These include four flux-limiter methods, two adaptive stencil methods, and one weighted stencil method.

3.1.1. Flux-limiter

Flux-limiter schemes satisfy many of the requirements of a good advection scheme. In particular, they are total variation diminishing (TVD), mass conservative and less diffusive than the simpler schemes (see for example, Harten [13] and LeVeque [15]). The accuracy of finite discretization is mainly related to the computation of the cell-face fluxes $\widehat{F}_{i+1/2}^n$. The most straightforward approximation to $\widehat{F}_{i+1/2}^n$ is certainly $\widehat{F}_{i+1/2}^n = 0.5u_{i+1/2}^n(Q_i^n + Q_{i+1}^n)$. This expression gives an approximation of the partial derivative $\partial u Q/\partial x$ by central differences. This method leads to the appearance of spurious oscillations in the numerical solution. One strategy to avoid non-physical oscillations and excessive numerical diffusion is the hybrid method which uses the second order numerical flux in smooth regions and limits the solution in vicinity of discontinuities by using the monotonic upwind method in these regions. This procedure is carried out by introducing a flux-limiter based on the local gradient of the solution. We write the interface value $Q_{i+1/2}^n$ as the sum of the diffusive first order upwind term and an “anti-diffusive” one. The higher order antidiffusive part is multiplied by the flux limiter, which depends locally on the nature of the solution by means of the non-linear function $\theta_{i+1/2}$. This function is expressed by the slope ratios at the neighborhood of the interfaces in the upwind direction:

$$\theta_{i+1/2} = \begin{cases} \frac{Q_i^n - Q_{i-1}^n}{Q_{i+1}^n - Q_i^n} = \theta_{i+1/2}^+ & \text{if } u_{i+1/2}^n \geq 0, \\ \frac{Q_{i+2}^n - Q_{i+1}^n}{Q_{i+1}^n - Q_i^n} = \theta_{i+1/2}^- & \text{if } u_{i+1/2}^n < 0. \end{cases} \tag{20}$$

Introduction of this new parameter namely (θ) and the limiter function Ψ , leads to the flux limiter version of the hybrid scheme as

$$Q_{i+1/2}^n = \begin{cases} Q_i^n + \frac{1}{2}(Q_{i+1}^n - Q_i^n)\Psi(\theta_{i+1/2}^+) & \text{if } u_{i+1/2}^n \geq 0, \\ Q_{i+1}^n - \frac{1}{2}(Q_{i+1}^n - Q_i^n)\Psi(\theta_{i+1/2}^-) & \text{if } u_{i+1/2}^n < 0. \end{cases} \tag{21}$$

The interface value $Q_{i-1/2}^n$ is obtained from $Q_{i+1/2}^n$, by replacing the index i with $i - 1$. From Eq. (21), one can see that if $\Psi = 0$ we find the upwind scheme, and if $\Psi = 1$ the scheme is reduced to the central one. The following limiter functions are used in this study [15]:

$$\begin{aligned} \text{Minmod : } & \Psi(\theta) = \max(0, \min(1, \theta)), \\ \text{Superbee : } & \Psi(\theta) = \max(0, \min(1, 2\theta), \min(2, \theta)), \\ \text{vanLeer : } & \Psi(\theta) = \frac{\theta + |\theta|}{1 + |\theta|}, \\ \text{MC : } & \Psi(\theta) = \max\left(0, \min\left(\frac{1 + \theta}{2}, 2, 2\theta\right)\right). \end{aligned} \tag{22}$$

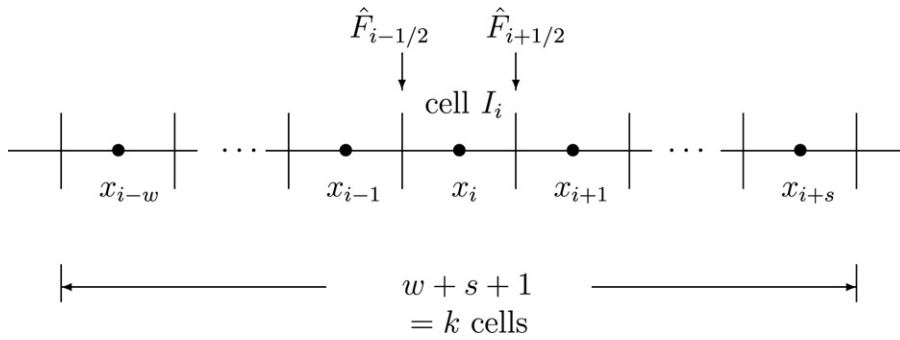


Fig. 3. Stencil $S_i^{(w)} = \{I_{i-w}, \dots, I_{i-1}, I_i, I_{i+1}, \dots, I_{i+s}\}$.

The Minmod and Superbee limiters were introduced by Roe [23] and Roe and Sidilkover [24]. The van Leer limiter was introduced in van Leer [27] and the monotized central (MC) limiter was also introduced by van Leer in a later paper [28].

3.1.2. Adaptive stencil (AS) methods

As depicted in Fig. 3, a formal definition of a cell (I_i) and a stencil (S_i) in the context of high resolution numerical methods is as follows: $I_i \equiv [x_{i-1/2}, x_{i+1/2}]$, $S_i^{(w)} = [I_{i-w}, I_{i-w+1}, \dots, I_i, I_{i+1}, \dots, I_{i+s}]$, $w = -1, 0, 1, \dots, k - 1$ where w and s represent the number of cells taken to the left and right of cell i , respectively, also referred to as the left and right stencil shift. The order of accuracy k on each stencil is related to w and s via the following relation: $k = w + s + 1$. If the same stencil is used for discretizing the partial differential equation at all grid cells I_i , then it is known that fixed stencil methods of second or higher order suffer from non-physical oscillations in the regions of discontinuity and in the neighborhood of steep fronts. As indicated by Shu [25], the paper of Harten et al. [14] directed the research toward an alternative approach, the adaptive stencil methods. The idea behind the adaptive stencil methods is to keep the total number of cells in the stencil constant, and to change the left shift w of the stencil if necessary with the coordinate x_i in order to avoid including the cell with the discontinuity in the interpolating polynomial. Thus, from a number of candidate stencils at each location x_i , the optimum stencil that results in the elimination of the numerical oscillation is chosen to approximate the flux.

3.1.2.1. SMIF method. The first adaptive stencil method used in this work is the hybrid monotonic difference scheme developed in Gushchin et al. [11,12], and Belotserkovskii [3] for the numerical simulation of fluid flows with large gradients of hydrodynamic parameters. The splitting on physical factors method for incompressible fluid flows (SMIF) is based on a combination of the modified central difference scheme MCDS and the modified upwind difference scheme MUDS with special switch condition. The splitting scheme is similar to the famous SMAC method of Amsden and Harlow [1], and to one of the approaches suggested in Fortin et al. [8]. It was shown that this hybrid scheme comes nearest to the third order schemes (Gushchin and Konshin [11]).

3.1.2.2. Essentially non-oscillatory (ENO) scheme. The second adaptive stencil method used in this work is the third order essentially non-oscillatory (ENO3) scheme. For the ENO scheme, as shown in Fig. 3, k candidate stencils can be defined at each cell I_i . On each of these stencils a k th order interpolation polynomial can be constructed:

$$\widehat{F}_{i+1/2}^{(w)} = \sum_{j=0}^{k-1} c_{w,j}^{(k)} F_{i-w+j}, \quad w = 0, \dots, k - 1,$$

where $k = 3$ for the ENO3 scheme. The coefficients $c_{w,j}^{(k)}$ can be found in Shu [25] for a fixed uniform grid. Smoothness indicators are used to estimate the smoothness of the solution. For $k = 3$ the smoothness indicators are given in Shu [25]. The stencil on which the interpolation is smoothest is then used for approximating the flux $\widehat{F}_{i+1/2}$.

3.1.3. Weighted stencil methods (WENO)

The WENO scheme is a weighted stencil method in which the idea is once again to define a number of candidate stencils at each grid location, but instead of selecting one of them for calculating the numerical flux, a convex combination of all candidate stencils is used. The advantage is that this method possesses k th order accuracy in the vicinity of discontinuities or steep fronts, and $(2k - 1)$ th order accuracy in smooth regions, where $k = w + s + 1$.

3.1.3.1. WENO5 scheme. The finite difference WENO5 scheme uses the same idea of applying ENO3 to construct cell faces of numerical fluxes. However, WENO5 uses a combination of 3 stencils $\{S_i^{(0)}, S_i^{(1)}, S_i^{(2)}\}$ or $\{S_i^{(-1)}, S_i^{(0)}, S_i^{(1)}\}$ for constructing interpolating polynomials depending on upwinding. If $(u_{i+1/2} > 0)$ (positive direction), the construction of $\hat{F}_{i+1/2}$ based on the 5th-order WENO5 scheme can be expressed as

$$\hat{F}_{i+1/2} = \sum_{w=0}^2 \omega_w f_{i+1/2}^{(w)}, \quad \omega_w = \frac{\alpha_w}{\sum_{l=0}^2 \alpha_l}, \quad \alpha_w = \frac{d_w}{(\epsilon - \beta^{(w)})^2}, \quad (d_0, d_1, d_2) = \left(\frac{3}{10}, \frac{3}{5}, \frac{1}{10}\right), \quad (23)$$

where $f_{i+1/2}^{(w)}$ approximates $\hat{F}_{i+1/2} = (uQ)_{i+1/2}$ using cell stencil $S_i^{(w)}$, $w = 0, 1, 2$ as shown in (24). The parameter $\epsilon = 10^{-6}$ is used to avoid a zero denominator:

$$\begin{aligned} f_{i+1/2}^{(0)} &= \frac{1}{3}F_i + \frac{5}{6}F_{i+1} - \frac{1}{6}F_{i+2}, & f_{i+1/2}^{(1)} &= -\frac{1}{6}F_{i-1} + \frac{5}{6}F_i + \frac{1}{3}F_{i+1}, \\ f_{i+1/2}^{(2)} &= \frac{1}{3}F_{i-2} - \frac{7}{6}F_{i-1} + \frac{11}{6}F_i, \end{aligned} \quad (24)$$

with the smoothness indicators $\beta^{(w)}$ given by

$$\begin{aligned} \beta^{(0)} &= \frac{13}{12}(F_i - 2F_{i+1} + F_{i+2})^2 + \frac{1}{4}(3F_i - 4F_{i+1} + F_{i+2})^2, \\ \beta^{(1)} &= \frac{13}{12}(F_{i-1} - 2F_i + F_{i+1})^2 + \frac{1}{4}(F_{i-1} - F_{i+1})^2, \\ \beta^{(2)} &= \frac{13}{12}(F_{i-2} - 2F_{i-1} + F_i)^2 + \frac{1}{4}(F_{i-2} - 4F_{i-1} + 3F_i)^2. \end{aligned} \quad (25)$$

3.2. Generalization for the multidimensional case

The generalization of the above finite-difference schemes to 2D and 3D problems is easily performed for convective terms as splitting mode in each one-dimensional direction. This way of extending the finite difference schemes is very simple and efficient, and hence is widely used in applications. However, such a generalization of the scheme to the multidimensional case can be only second order accurate for general nonlinear systems regardless of the order of accuracy in the one-dimensional procedure (as pointed out by Zhang et al. [35]).

4. Results

In this section we are comparing the performance of the high-order upwind schemes for the unsteady problem of the collapse of a mixed region in a linearly stratified fluid. Due to symmetry, the solution of problem (1)–(7) was sought in the first quadrant ($x \geq 0$ and $z \geq 0$) of the plane (x, z) with the symmetry conditions at $x = 0$ and $z = 0$. When solving the problem considered, the zero conditions at infinity were shifted and formulated at the boundary of a sufficiently large rectangular region. Variables are discretized on a uniform rectangular grid of mesh size Δx and Δz in the horizontal and vertical directions, respectively. The three different grids with $\Delta x = \Delta z = 0.1$, $\Delta x = \Delta z = 0.05$, and $\Delta x = \Delta z = 0.025$, are used to estimate rate of convergence. Order of accuracy is based on the ratio of errors from the two finest grids. The convergence rate of the flux-limiter schemes is a little less than 2nd-order. The convergence rate of SMIF, ENO3 and WENO5 is a little better than 2nd-order. These results are in agreement with the comments of Zhang et al. [35] that the ENO and WENO schemes are only 2nd-order accurate for a general nonlinear system, regardless of the order of accuracy in the one dimensional reconstruction procedure. The selection of a suitable domain size is based on a straightforward analysis in which the size of the domain is systematically increased until its effect on prediction

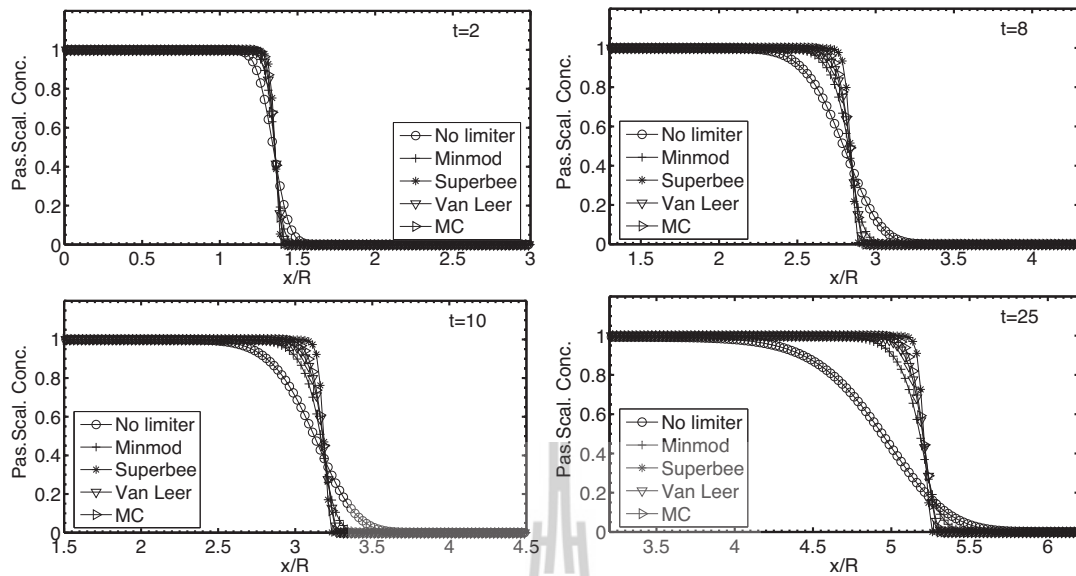


Fig. 4. Profiles of passive scalar concentrations at transect $z = 0.5\Delta z$ ($C(t, x, 0.5\Delta z)$). Four flux-limiter schemes are compared in the case of $Re = 10^3$, $\Delta x = \Delta z = 0.05$, $\Delta t = 0.001$, (o) no limiter (first order monotone scheme), (+) Minmod, (*) Superbee, (∇) van Leer, and (\triangleright) MC.

becomes small. A domain of length $x^* \simeq 10R$ and height $z^* \simeq 4R$ was found reasonable for the time interval considered. In his laboratory experiment, Wu [33] examined in detail the collapse of the original mixed region and the growth and propagation of internal waves. The process of collapse can be divided into initial, principal and final collapse stages. At the first two stages, the collapse is a gravitation flow phenomenon. Empirical formulae have been derived to describe the process of the first two stages. A nearly constant rate of collapse is found for the initial stage. The rate of wake collapse slows down gradually at the principal collapse stage. At the final stage, the collapse slows down even further with increasing viscous effects. We used the data of Wu [33] as a benchmark test to compare performance of the different numerical approaches.

4.1. Width, profiles and areas of collapsing region

The profiles of the collapsing region were traced from the evolution of the passive scalar concentration and from the evolution of Lagrangian particles' positions. The finite difference schemes have different smearing of the density and passive scalar concentration discontinuities. The best way to define the evolution of mixing zone size is to draw and analyze profiles of passive scalar concentration at different transects. These results are shown clearly in Figs. 4 and 5 in which we present a transect $z = 0.5\Delta z$ of the numerical solution for passive scalar concentration. Fig. 4 shows the graphs of transect $z = 0.5\Delta z$ for different moments of time. Here we compare upwind (no flux-limiter) scheme with four flux-limiter schemes given by Eq. (22). The first order upwind scheme smears the solution too much (see lines marked by circle signs). The limiter schemes reduce the numerical diffusion as compared to the upwind scheme. Comparing the performance of MC and van Leer limiters (lines marked by the right triangle ' \triangleright ' and down triangle ' ∇ ' signs) nearly identical results are seen and a negligible numerical diffusion is introduced compared to the one introduced by Minmod limiter (lines marked by plus '+' signs). The Superbee limiter (lines marked by star '*' signs) gives better results with regards to limiting of the numerical diffusion.

Fig. 5 shows the graphs of $C(t, x, 0.5\Delta z)$ for different instances of time. Here we compare the four schemes – the Superbee flux-limiter, the SMIF, the ENO3 and the WENO5. For time interval up to $t \simeq 4$ there is almost no difference in performance. For larger times $t \gtrsim 6$ the Superbee limiter gives the smallest numerical diffusion compared with SMIF, ENO3 and WENO5. Performance of ENO3 and SMIF are nearly identical as seen from

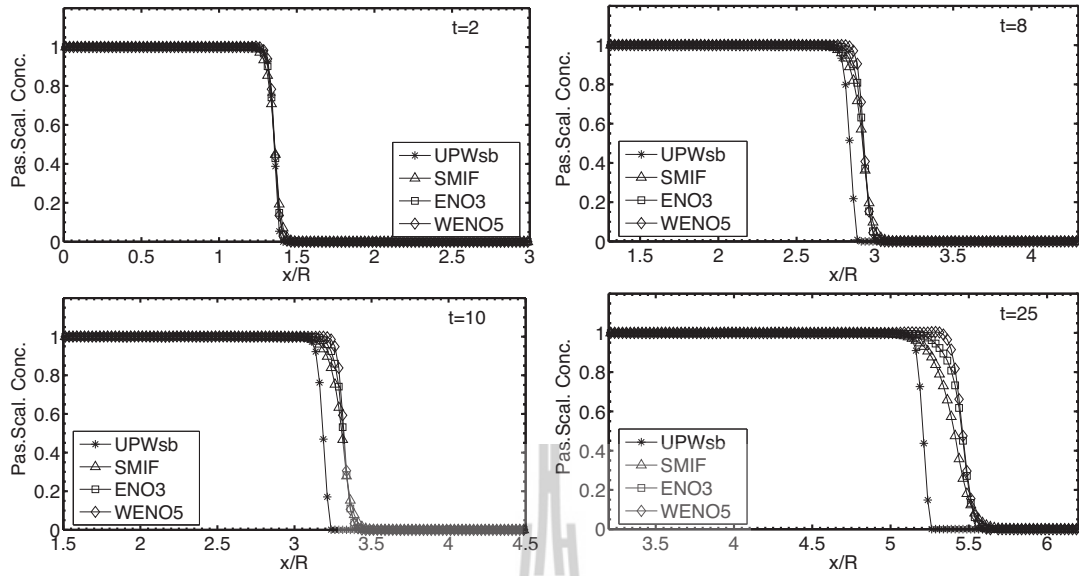


Fig. 5. Profiles of passive scalar concentrations at transect $z = 0.5\Delta z$ ($C(t, x, 0.5\Delta z)$). Four approximations of convective terms are compared in the case of $Re = 10^3$, $\Delta x = \Delta z = 0.05$, $\Delta t = 0.001$, (*) flux-limiter Superbee (UPWsb), (Δ) SMIF, (\square) ENO3, and (\diamond) WENO5.

data in Fig. 5 up to time $t \approx 10$. Scheme WENO5 produces less numerical diffusion compared with ENO3 and SMIF.

Fig. 6 illustrates the temporal history of the mixed region width for the four calculations using flux-limiter Superbee (UPWsb) Fig. 6(a), SMIF (b), ENO3 (c), and WENO5 (d). The stars and triangles are the results of the numerical simulations computed herein. The star signs represent the position $C(t, x^*, 0.5\Delta z) = 0.01$ of passive scalar concentration and the triangle signs represent the position $C(t, x^\Delta, 0.5\Delta z) = 0.99$. The dashed line is drawn according to Wu’s [33] original experimental data. The solid curve is made up of two functions:

$$\frac{x}{R} = 1 + 0.29(t/T)^{1.08} \quad \text{for } 0 \leq \frac{t}{T} \leq 2.75, \tag{26}$$

$$\frac{x}{R} = 1.03(t/T)^{0.55} \quad \text{for } 2.75 \leq \frac{t}{T} \leq 25,$$

which were found by Wu to fit his experimental data. Fig. 6 shows the drawn for $Re = 10^3$, $\Delta x = \Delta z = 0.05$, time increment was $\Delta t = 0.001$. Our numerical results match Wu’s experimental data reasonably well (dashed curve in Fig. 6). The data in Fig. 6 show that the upwind scheme with Superbee limiter (UPWsb) gives a width of the mixed region which is smaller than Wu’s experimental data, but at the same time this scheme has smallest numerical diffusion and as a result numerical smearing of the discontinuity of the concentration of passive scalar ($x^* - x^\Delta$) is smallest. The ENO3 and SMIF schemes reproduced the width of the mixed region nearly identically. The WENO5 scheme gives results closer to Wu’s experimental data. Figs. 7–10 show Lagrangian particle distributions and contours of the passive scalar concentration at different time instants for the case of $Re = 5 \times 10^4$. Computations were performed on the grid 360×160 with $\Delta x = \Delta z = 0.05$. The time step was $\Delta t = 0.001$. There were 8050 particles in the mixed region at the initial instant. The shaded domain represents the shape of the mixed region defined by the Lagrangian particles. To make this region transparent we have not drawn all the particles. The solid lines in Figs. 7–10 show the evolution of the curve $C(t, x, z) = const$. Lines with letter “a” represent level $C(t, x, z) = 0.01$, lines with letter “b” represent level $C(t, x, z) = 0.5$ and lines with letter “c” represent $C(t, x, z) = 0.99$. In Fig. 7, we compare the results of five schemes; the first order upwind and the four schemes with flux limiters given by Eq. (22) at time $t = 4$. It can be seen that the Superbee limiter scheme has the smallest dispersion of the passive scalar concentration. If the shape of the mixed region is defined by the contour line $C(t, x, z) = const$. then the contour level $C(t, x, z) = 0.5$ coincides with shape of a mixed region defined by the Lagrangian particles. Contour lines $C(t, x, z) = 0.01$ define a large domain of the

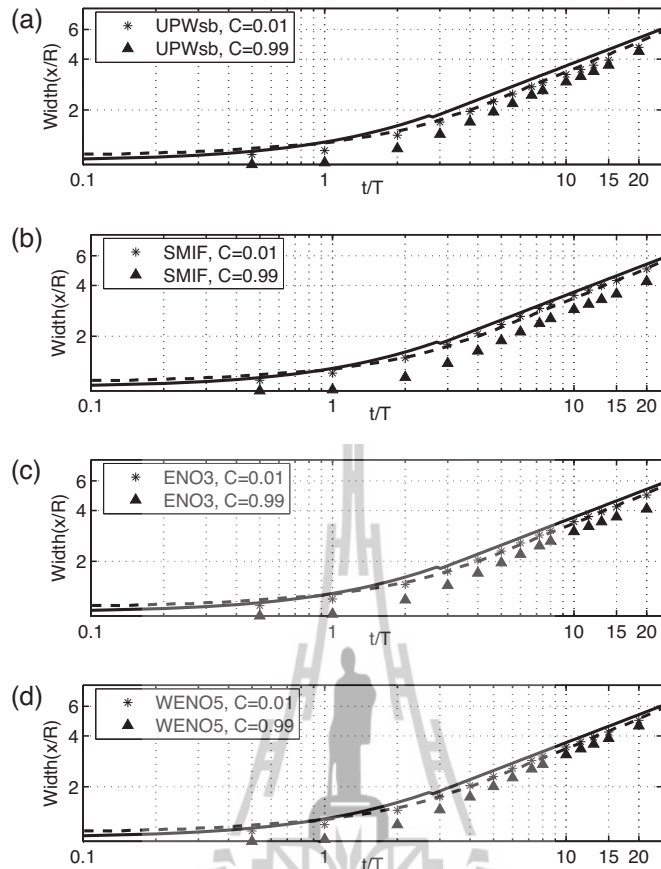


Fig. 6. Comparisons with Wu's data $Re = 10^3$, $\Delta x = \Delta z = 0.05$, $\Delta t = 0.001$. Flux-limiter Superbee (UPWsb) (a); SMIF (b); ENO3 (c); WENO5 (d); (*) corresponds to $C(t, x^*, 0.5\Delta z)$; (\blacktriangle) corresponds to $C(t, x^*, 0.5\Delta z)$; solid lines represent formulae (26), (dashed) Wu's experimental data [33].

mixed region compared with the region defined by the Lagrangian particles. Contour lines, $C(t, x, z) = 0.99$, are located inside the shaded region for every time instant presented in Figs. 7–10. Cross signs (\times) on the x -axis correspond to the width of the mixed region according to Wu's experiments. It can be seen that contour lines $C(t, x, z) = 0.01$ define the width of the mixed region corresponding to the experimental data. The width of the mixed region defined by a tracer particle for all schemes is smaller than the experimental results of Wu.

In Fig. 8, we compare the results of four schemes, namely the scheme with Superbee flux-limiter, two adaptive stencil schemes (SMIF and ENO3), and a weighted stencil scheme (WENO5) at time $t = 4$. Performance of the adaptive stencil schemes and weighted stencil scheme are almost identical. We can see that the curve $C(t, x, z) = 0.5$ coincides with the edge of the shaded region. The scheme with Superbee limiter demonstrates a smaller value of the mixed region width compared with SMIF, ENO3 and WENO5.

Figs. 9 and 10 show results of comparison of the four schemes (Superbee, SMIF, ENO3 and WENO5) at the time instants $t = 10, 20$. The qualitative behaviour is similar to the previous case corresponding to $t = 4$. Curve $C(t, x, z) = 0.5$ corresponds to the edge of the shadowed domain. The width of the mixed region defined by Lagrangian particles is smaller than Wu's experimental results.

Comparison of results for $Re = 10^3$ and $Re = 5 \times 10^4$ demonstrate a weak dependence on the Reynolds number. It was pointed out by [33] that the collapse during the initial ($t \approx 3$) and principal stages ($3 < t < 25$) is primarily a gravitational flow phenomenon, and that the collapse process during these stages is almost identical for different Reynolds numbers. Note that in case of $Re = 10^3$ the computational domain was $10R \times 4R$ in x and z directions, respectively. In case of $Re = 5 \times 10^4$ the computational domain was approximately twice larger, $18R \times 8R$, in the x and z directions, respectively.

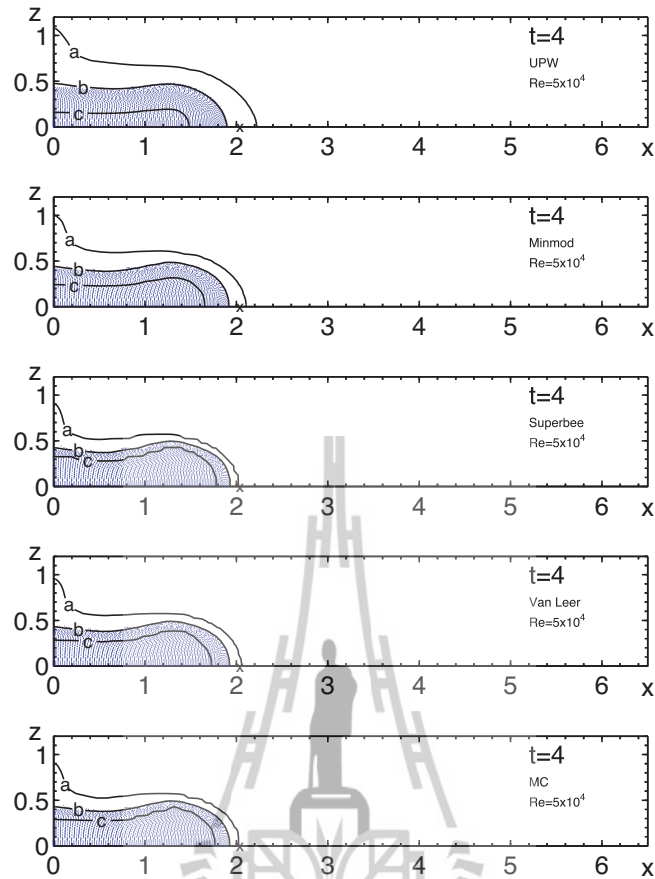


Fig. 7. Shapes of the collapsed mixed region at time $t=4$ of 1st-order UPW and four flux-limiters, solid lines represent contour lines from numerical results of passive scalar concentration, shaded areas represent mixed region taken from Lagrangian particles. $Re = 5 \times 10^4$, $\Delta x = \Delta z = 0.05$ and $\Delta t = 0.001$.

This note demonstrates that the size of computational domain $10R \times 4R$ is sufficient to shift boundary conditions from infinity to the boundary of the computational domain.

4.2. Internal wave generated by collapsing region

The experiments of [33] represent the pattern of internal waves generated by the collapse of the mixed region in the stratified fluid.

The results presented in this section correspond to $Re = 5 \times 10^4$, which is the same as in Wu’s experiment. The total computational domain size, compared to the radius of the initial mixed region, is 18 radii wide and 8 radii high. We used a uniform mesh with grid spacings $\Delta x = \Delta z = 0.05$. Fig. 11 shows constant density lines at successive time instants. Fig. 11 shows in detail the collapse of the original mixed region and the growth and propagation of internal waves. During the initial collapse of the mixed region, $t \leq 4$, the fluid layers near the axis $x=0$ displace toward the center of mixed region ($x=0, z=0$) and reach their maximum deflection at the end of the initial collapse stage. As the deflected layers oscillate back toward their equilibrium positions, undulations of the isopycnic lines are observed.

In order to better understand the wave generated by a collapsing region, the phase pattern of internal waves is illustrated in Fig. 12, where isolines $\partial \rho_1 / \partial x = const$ are drawn at time instants $t=2, 4, 10,$ and 20 . Lines $\partial \rho_1 / \partial x = 0$ correspond to peaks and troughs of internal waves. Not far from the center, except for the small region where the

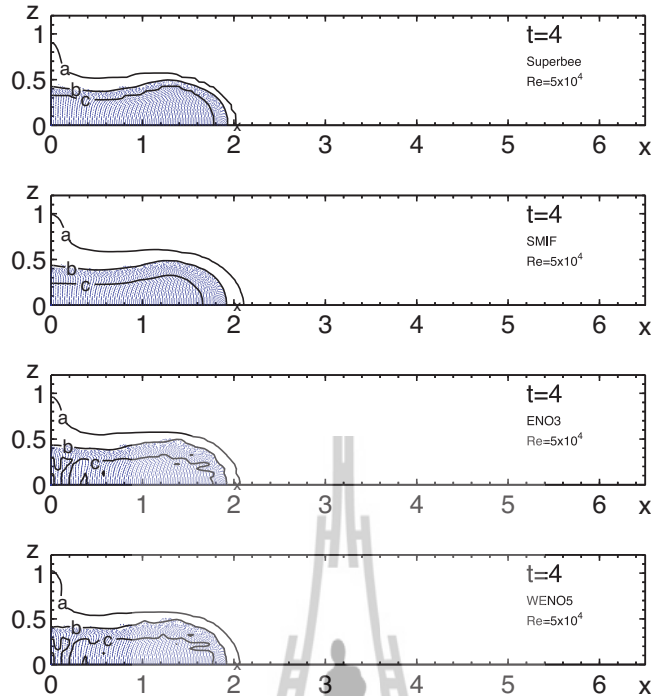


Fig. 8. Shapes of the collapsed mixed region at time $t = 4$ of Superbee, SMIF, ENO3 and WENO5, solid lines represent contours line from numerical results of passive scalar concentration, shaded areas represent mixed region taken from Lagrangian particles. $Re = 5 \times 10^4$, $\Delta x = \Delta z = 0.05$ and $\Delta t = 0.001$.

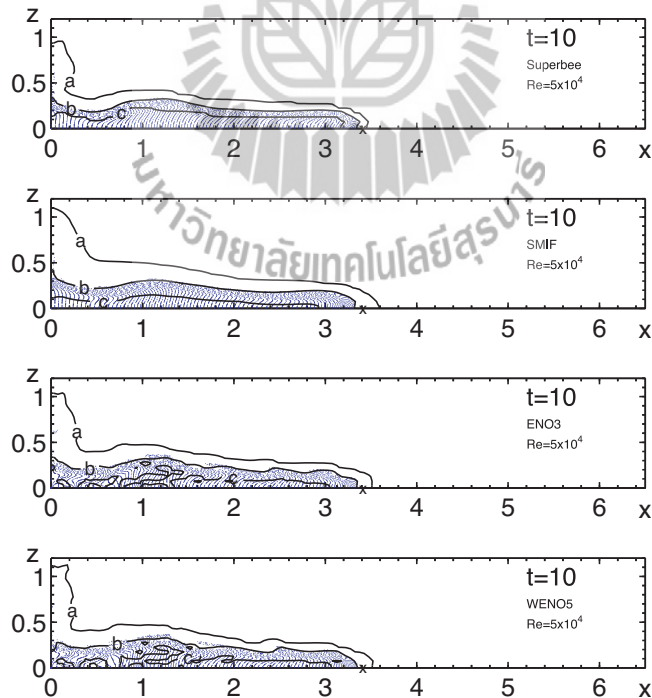


Fig. 9. Shapes of the collapsed mixed region at time $t = 10$ of Flux-limiter/Superbee, SMIF, ENO3 and WENO5, solid lines represent contour lines from numerical results of passive scalar concentration, shaded areas represent mixed region taken from Lagrangian particles. $Re = 5 \times 10^4$, $\Delta x = \Delta z = 0.05$ and $\Delta t = 0.001$.

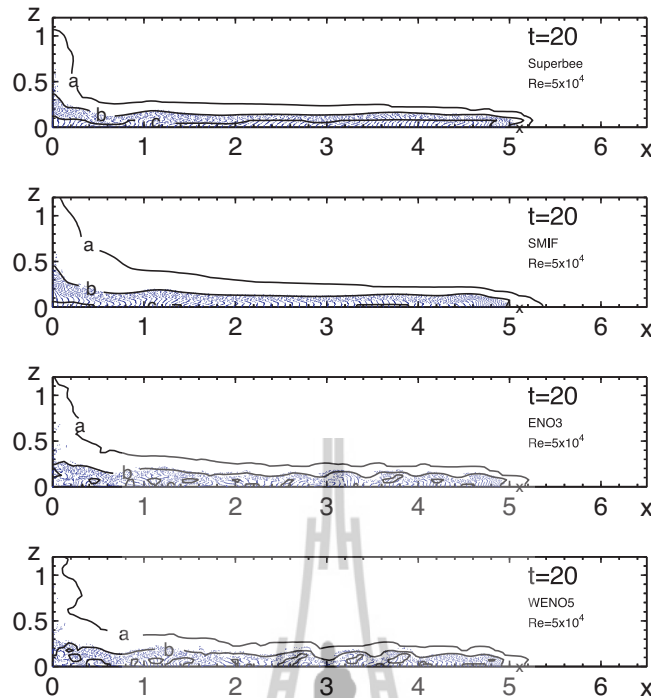


Fig. 10. Shapes of the collapsed mixed region at time $t=20$ of Flux-limiter/Superbee, SMIF, ENO3 and WENO5, solid lines represent contour lines from numerical results of passive scalar concentration, shaded areas represent mixed region taken from Lagrangian particles. $Re=5 \times 10^4$, $\Delta x = \Delta z = 0.05$, and $\Delta t = 0.001$.

finite size of mixed region is dominant, these lines are almost straight. This agrees with the experimental data of [33]. However, for large distance from the center, the lines $\partial \rho_1 / \partial x = 0$ change to a curve. This behavior of phase lines $\partial \rho_1 / \partial x = 0$ does not relate to the method of approximation of convective terms. Other approximations of convective terms used in this work demonstrate similar effects.

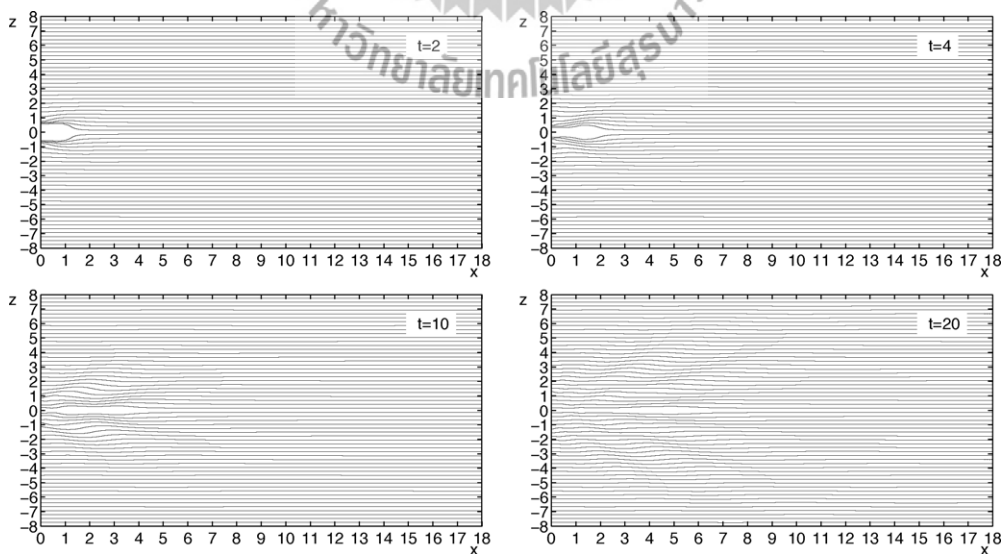


Fig. 11. The constant density lines, $\rho(t, x, z) = \text{const}$, at successive time intervals. Results from SMIF approximation of convective terms are presented for $Re=5 \times 10^4$, $\Delta x = \Delta z = 0.05$, $\Delta t = 0.001$.

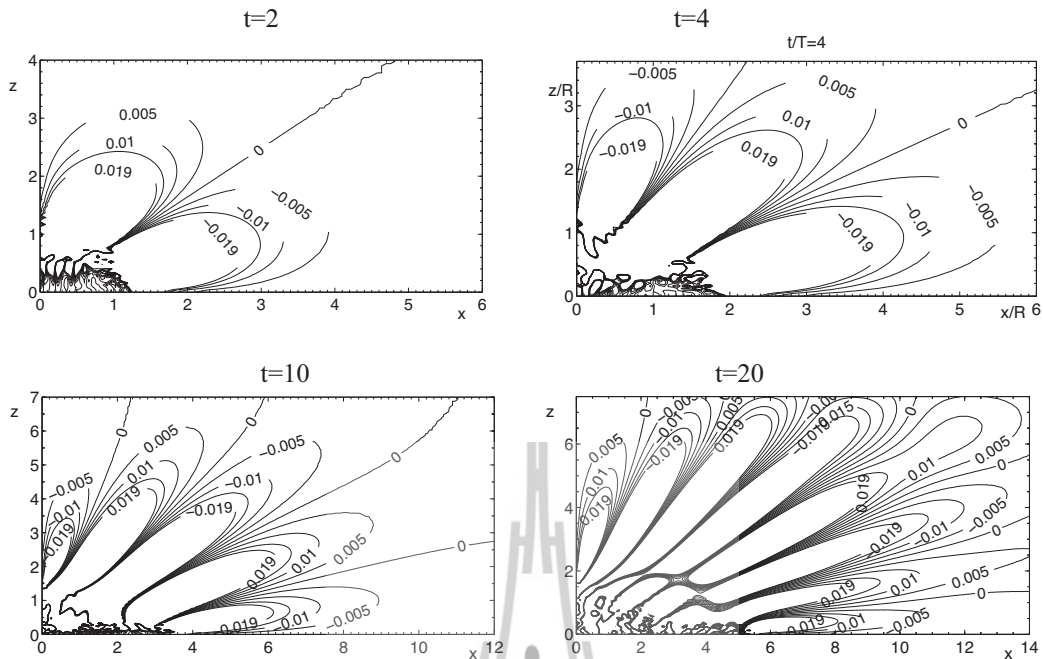


Fig. 12. Isolines $\partial\rho_1/\partial x = \text{const.}$ Computational results from WENO5 approximation of convective terms with $Re = 5 \times 10^4$, $\Delta x = \Delta z = 0.05$ and $\Delta t = 0.001$.

5. Conclusions and future works

Numerical simulations of the collapse of a fully mixed region in a linearly stratified fluid were considered. The simulations are based on the incompressible Navier–Stokes equations in the Oberbeck–Boussinesq approximation. Three groups of high-order monotone finite difference schemes have been successfully tested and compared within this problem.

1. The flux-limiter schemes used a ‘fixed’ stencil and demonstrated reasonable accuracy and had small numerical diffusion. The Superbee limiter had smallest smearing of discontinuity, is not recommended for the problem considered because it significantly reduces the convection velocity of discontinuity.
2. Two schemes with ‘adaptive’ stencil are ENO3 and SMIF. They obey small numerical diffusion and results obtained using these schemes are in good agreement with experimental data.
3. The WENO5 scheme is a ‘weighted’ stencil method. The WENO5 does better reproduce experimental data compared with the other methods used in this paper. Because the WENO5 scheme used a stencil which contains discontinuity we observed small dispersion in the area of discontinuity.

From the results of numerous computational tests, some recommendations can be made. To reproduce the initial stage of collapse of the mixed region all considered schemes gave sufficiently accurate results. For large time of collapse, SMIF, ENO3 or WENO5 scheme have to be used.

A more significant influence of different high-order upwind approximations on the pattern of the internal waves is observed for waves with density level corresponding to the density of unperturbed fluid on the levels of the mixed region.

The work reported in this paper is the very beginning stage of a project whose ultimate goal is the development of a numerical model applicable to the realistic geophysical flows in natural environment. Planned work includes extension of numerical model to flows in media with nonlinear stratification and to a large time of degeneration corresponding the final stage of collapse.

Acknowledgements

This research was partially supported by Suranaree University of Technology, by the Higher Education Research Promotion and National Research University Project of Thailand, Office of the Higher Education Commission and by Russian Foundation for Basic Research (RFBR-10-01-00435).

References

- [1] A.A. Amsden, F.H. Harlow, The SMAG Method, Los Alamos Scient. Lab. Rept., 1970, LA-4370.
- [2] A.V. Babakov, Application of flow theory to a problem of the dynamics of a viscous stratified fluid, *USSR Computational Mathematics and Mathematical Physics* 23 (2) (1983) 115–119.
- [3] O.M. Belotserkovskii, *Mathematical Modelling in Informatics: Numerical Simulation in the Mechanics of Continuous Media*, Moscow, Russia, 1997.
- [4] D. Brown, R. Cortez, M.I. Minion, Accurate projection methods for the incompressible Navier–Stokes equations, *Journal of Computational Physics* 168 (2001) 464–499.
- [5] G.G. Chernykh, O.F. Voropaeva, On numerical modelling of local density perturbation dynamics using moving grids, *Journal of Engineering Thermophysics* 20 (3) (2011) 290–301.
- [6] S.K. Godunov, A difference scheme for numerical solution of discontinuous solution of hydrodynamic equations, *Matematicheskii Sbornik* 47 (1959) 271–306 (translated US Joint Publ. Res. Service, JPRS 7226, 1969).
- [7] N. Fedorov, *Fine Thermohaline Structure of Oceanic Water*, Gidrometeoizdat, Leningrad, 1976 (in Russian).
- [8] M. Fortin, R. Peyret, R. Temam, Résolutions numériques des équations de Navier–Stokes pour un fluide incompressible, *Journal de Mécanique* 3 (10) (1971) 357–390.
- [9] H.E. Gilreath, A. Brandt, Experiments on the generation of internal waves in a stratified fluid, *AIAA Journal* 23 (1985) 693–700.
- [10] V.A. Gushchin, The splitting method for problems of the dynamics of an inhomogeneous viscous incompressible fluid, *USSR Computational Mathematics and Mathematical Physics* 21 (4) (1981) 190–204.
- [11] V.A. Gushchin, V.N. Konshin, Computational aspects of the splitting method for incompressible flow with a free surface, *Computers & Fluids* 21 (1992) 345–353.
- [12] V.A. Gushchin, P.V. Matyushin, Numerical simulation of separated flow past a sphere, *Computational Mathematics and Mathematical Physics* 37 (1997) 1086–1100.
- [13] A. Harten, High-resolution schemes for hyperbolic conservation laws, *Journal of Computational Physics* 49 (1983) 357–393.
- [14] A. Harten, B. Engquist, S. Osher, S. Chakravarthy, Uniformly high order accurate essentially non-oscillatory schemes, III, *Journal of Computational Physics* 71 (1987) 231–303.
- [15] R.J. LeVeque, High-resolution conservative algorithms for advection in incompressible flow, *SIAM Journal on Numerical Analysis* 33 (1996) 627–665.
- [16] J. Lighthill, *Waves in Fluids*, 2nd ed., Cambridge University Press, Cambridge, UK, 2001.
- [17] Yu.M. Lytkin, G.G. Chernykh, On internal waves induced by the mixing zone collapse in a stratified fluid, in: *Mathematical Problems of Mechanics (Continuum Dynamics)*, vol. 22, Inst. of Hydrodynamics, Sib. Branch USSR Akad. Sci., Novosibirsk, 1975, pp. 116–132 (in Russian).
- [18] V.S. Maderich, V.I. Nikishov, A.G. Stetsenko, *Internal Mixing Dynamics in a Stratified Medium*, Naukova Dumka, Kiev, 1988 (in Russian).
- [19] A.S. Monin, R.V. Ozmidov, *Oceanic Turbulence*, Gidrometeoizdat, Leningrad, 1981 (in Russian).
- [20] N.P. Moshkin, G.G. Chernykh, A.V. Fomina, On the influence of small total momentum imbalance on turbulent wake dynamics in the linearly stratified medium, *Matematicheskoe Modelirovanie* 17 (1) (2005) 19–33.
- [21] J.R. Munroe, C. Voegeli, B.R. Sutherland, V. Birman, E.H. Meiburg, Intrusive gravity currents from finite-length locks in a uniformly stratified fluid, *Journal of Fluid Mechanics* 635 (2009) 245–273.
- [22] V.P. Nartov, G.G. Chernykh, On Numerical Modelling of Fluid Flow Generated by Collapse of Mixed Region in Stratified Medium, Preprint, Institute of Theoretical and Applied Mechanics, Novosibirsk, 1982 (in Russian).
- [23] B. Roe, Some contributions to the modeling of discontinuous flows, *Lecture Notes on Applied Mathematics* 22 (1985) 163–193.
- [24] B. Roe, D. Sidilkover, Optimum positive linear schemes for advection in two and three dimensions, *SIAM Journal on Numerical Analysis* 29 (1992) 1542–1568.
- [25] C.-W. Shu, Essentially non-oscillatory and weighted essentially nonoscillatory schemes for hyperbolic conservation laws, in: A. Quarteroni (Ed.), *Advanced Numerical Approximation of Nonlinear Hyperbolic Equations*, vol. 1697, Springer-Verlag, Berlin, 1998, pp. 325–432.
- [26] J.S. Turner, *Buoyancy Effects in Fluids*, Cambridge University Press, Cambridge, 1973.
- [27] B. Van Leer, Towards the ULTIMATE conservation difference scheme. II. Monotonicity and conservation combined in a second order scheme, *Journal of Computational Physics* 14 (1974) 361–370.
- [28] B. Van Leer, Towards the ULTIMATE conservation difference scheme. IV. A new approach to numerical convection, *Journal of Computational Physics* 23 (1977) 276–299.
- [29] O.F. Voropaeva, G.G. Chernykh, Internal waves generated by momentumless turbulent wake in a linearly stratified fluid, *Matematicheskoe Modelirovanie* 10 (6) (1998) 75–89.
- [30] O.F. Voropaeva, N.P. Moshkin, G.G. Chernykh, Internal waves generated by turbulent wakes in a stably stratified medium, *Doklady Physics* 48 (9) (2003) 517–521.

- [31] E.V. Vorozhtsov, N.N. Yanenko, *Methods for the Localization of Singularities in Numerical Solutions of Gas Dynamics Problems*, Springer-Verlag, New York, 1989.
- [32] W.R. Wessel, Numerical study of the collapse of a perturbation in an infinite density-stratified fluid, *Physics of Fluids* 12 (12, Pt II) (1969) 170–176.
- [33] J. Wu, Mixed region collapse with internal wave generation in a density-stratified medium, *Journal of Fluid Mechanics* 35 (Pt 3) (1969) 531–544.
- [34] N.N. Yanenko, *The Method of Fractional Steps. The Solution of Problems of Mathematical Physics in Several Variables*, Springer, New York, 1971.
- [35] R. Zhang, M. Zhang, C.-W. Shu, On the order of accuracy and numerical performance of two classes of finite volume WENO schemes, *Computer Physics Communications* 9 (2011) 807–827.

